TN-2244

NATIONAL ADVISORY COMMITTEE FOR AERONAUTICS

TECHNICAL NOTE 2244

A COMPARISON OF THEORY AND EXPERIMENT FOR

HIGH-SPEED FREE-MOLECULE FLOW

By Jackson R. Stalder, Glen Goodwin,
and Marcus O. Creager

Ames Aeronautical Laboratory
Moffett Field, Calif.

NACA

Washington
December 1950

NATIONAL ADVISORY COMMITTEE FOR AERONAUTICS

TECHNICAL NOTE 2244

A COMPARISON OF THEORY AND EXPERIMENT FOR

HIGH-SPEED FREE-MOLECULE FLOW

By Jackson R. Stalder, Glen Goodwin,
and Marcus O. Creager

SUMMARY

A comparison is made of free-molecule-flow theory with the results
of wind-tunnel tests performed to determine the drag and temperature-
rise characteristics of a transverse circular cylinder.

The model consisted of a 0.0031-inch-diameter cylinder constructed
of butt-welded iron and constantan wires. Temperatures were measured at
the center and both ends of the model. The cylinder was tested under
conditions where the Knudsen number of the flow (ratio of mean-free-
molecular path to cylinder radius) varied between 4 and 185. The molec-
ular speed ratio (ratio of stream speed to the most probable molecular
speed) varied from 0.5 to 2.3. In terms of conventional flow parameters,
these test conditions corresponded to a Mach number range from 0.55 to
2.75 and a Reynolds number range from 0.005 to 0.90.

The measured values of the cylinder center-point temperature con-
firmed the salient point of the heat-transfer analysis which was the
prediction that an insulated cylinder would attain a temperature higher
than the stagnation temperature of the stream.

Good agreement was obtained between the theoretical and the experi-
mental values for the drag coefficient. As predicted, theoretically,
the drag coefficient was independent of Knudsen (or Reynolds number)
variation and depended primarily upon the molecular-speed ratio.

INTRODUCTION

The various phenomena connected with the high-speed flows of rare-
fied gases have recently been the subject of several analytic investi-
gations (references 1, 2, 3, and 4). Interest in this phase of aero-
dynamics and thermodynamics has been aroused primarily because of the
necessity of being able to compute forces on and heat transfer to mis-
siles which may fly at great altitudes at high speed. In another
analytic exploration of this field, simplified concepts of aerodynamic
and thermodynamic phenomena occurring at high altitudes have been used

by Whipple (reference 5) in an investigation of the properties of the upper atmosphere by means of measurements of the brightness and deceleration of meteors.

Experimental work in the field of high-speed rarefied gas flows has been practically nonexistent up to this point. The pioneer work of Epstein (reference 6) on the drag of spheres in a rarefied gas was concerned only with very low-speed motions. Consequently, the purpose of the present investigation was twofold: (1) to obtain experimental data that could be compared with the predictions of an analytic treatment of aerodynamic and thermodynamic processes occurring at very high altitudes; and (2) as a means to this end, to develop a wind-tunnel and related instrumentation that would permit testing of models under simulated conditions of high-altitude high-speed flight. In connection with the second objective — the development of a wind tunnel and instrumentation — it should be pointed out that a low-density wind tunnel is being developed concurrently at the University of California and the authors wish to acknowledge the assistance they have received from the reports issued by this group, as well as the stimulus received from conversations with the University of California personnel.

At the beginning of the experimental work, it was decided that the initial model tests in the low-density wind tunnel should be confined to the free-molecule-flow regime despite the fact that this regime is probably of less technical importance than the slip-flow and intermediate regimes. This decision was reached because the free-molecule regime is susceptible to analysis; whereas the slip-flow and intermediate regimes have not yet been adequately treated (cf., reference 2). In view of the many uncertainties connected with the development of entirely new types of wind-tunnel instrumentation, it was thought to be essential to test in a field where the experimental work could be guided by a theoretical background.

The selection of the test body was governed both by the requirement that free-molecule flow be obtained and by the practical considerations arising from tunnel size and instrumentation. The former condition required that the significant body dimension be small compared to the mean-free-molecular path.

A cylinder with axis perpendicular to the stream was chosen as the body which most nearly fulfilled the requirements of the test. The radius of the cylinder could be made small compared with the mean-free path. In addition, since it was desired to measure both aerodynamic forces and body temperature, the cylinder had the virtue of being doubly symmetrical so that only drag force had to be measured. The problem of temperature measurement could be solved by constructing the model from dissimilar metals so that the model itself formed a thermocouple.

The present investigation is a first step toward an attempt to gain an understanding of the comparatively new and unexplored field of

high-speed low-density flows. The experiments reported herein were made to provide a comparison with some important results of free-molecule-flow theory and to facilitate the solution of problems connected with the design, operation, and instrumentation of a low-density wind tunnel. The tests were conducted in the Ames low-density wind tunnel.

NOTATION

A surface area, square feet

$\left.\begin{array}{c} c_x \\ c_y \\ c_z \end{array}\right\}$ components of total velocity, feet per second

C_D total drag coefficient, dimensionless

C_{D_i} impinging drag coefficient, dimensionless

C_{D_r} re-emission drag coefficient, dimensionless

D total drag force, pounds

E_i rate of incident molecular energy, foot-pounds per second

E_r rate of re-emitted molecular energy, foot-pounds per second

E_R rotational energy, foot-pounds per molecule

E_t rate of incident translational molecular energy on front side of body, foot-pounds per second

$f(s)$ dimensionless function of s defined by $f(s) = Z_1(s^2+3) + Z_2\left(s2+\dfrac{7}{2}\right)$

$f^o(s)$ dimensionless function of s defined by $f^o(s) = Z_1(s2+2) + Z_2\left(s2+\dfrac{5}{2}\right)$

$g(s)$ dimensionless function of s defined by $g(s) = 3(Z_1+Z_2)$

$g^o(s)$ dimensionless function of s defined by $g^o(s) = 2(Z_1+Z_2)$

G normal force, pounds

I_o modified Bessel function of first kind and zero order

I_1 modified Bessel function of first kind and first order

J mechanical equivalent of heat, 778 foot-pounds per Btu

k Boltzmann constant, 5.66×10^{-24} foot-pounds per ^oF per molecule

K   Knudsen number (ratio of mean-free-molecular path to cylinder
           radius), dimensionless

$\left.\begin{array}{l} l_x \\ l_y \\ l_z \end{array}\right\}$ direction cosines, dimensionless

L   length, feet

m   mass of one molecule, slugs

M   Mach number, dimensionless

n   number of molecules striking body, molecules per square foot,
           second

N   number of molecules per unit volume of gas

p   free-stream static pressure, pounds per square foot

r   cylinder radius, feet

R   universal gas constant, 1544 foot-pounds per pound-mole,
           $^\circ F$ absolute

s   molecular-speed ratio, (ratio of stream mass velocity to most
           probable molecular speed), dimensionless

T   free-stream static temperature, $^\circ F$ absolute

T_O tunnel stagnation temperature, $^\circ F$ absolute

T_c cylinder temperature, $^\circ F$ absolute

T_w surface temperature, $^\circ F$ absolute

T_t test-section wall temperature, $^\circ F$ absolute

U   mass velocity, feet per second

$\left.\begin{array}{l} U_x \\ U_y \\ U_z \end{array}\right\}$ components of mass velocity, feet per second

v_r re-emission velocity, feet per second

v_m most probable molecular speed, feet per second

W   molecular weight, pounds per pound-mole

$\left.\begin{array}{l} x \\ y \\ z \end{array}\right\}$ Cartesian coordinates

Z_1 dimensionless function of s defined by $Z_1 = \pi e^{-s^2/2} I_0(s^2/2)$

Z_2 dimensionless function of s defined by

$$Z_2 = \pi s^2 e^{-s^2/2} \left[I_0(s^2/2) + I_1(s^2/2) \right]$$

α accommodation coefficient, dimensionless

β reciprocal of most probable molecular speed, seconds per foot

Γ gamma function

γ ratio of specific heats, dimensionless

ϵ emissivity, dimensionless

θ angle of body element with respect to free stream, radians

ρ density of free stream, slugs per cubic foot

σ Stefan–Boltzmann constant, 3.74×10^{-10} foot–pounds per square
       foot, $^\circ F^4$

ψ dimensionless group defined by

$$\psi = 1 + \frac{1 + \frac{3\sqrt{\pi}}{2} s \sin \theta \left[1 + \mathrm{erf}\,(s \sin \theta)\right] e^{s^2 \sin^2 \theta}}{1 + \sqrt{\pi}\ s \sin \theta \left[1 + \mathrm{erf}\,(s \sin \theta)\right] e^{s^2 \sin^2 \theta}}$$

ψ' dimensionless group defined by

$$\psi' = 1 + \frac{1 - \frac{3\sqrt{\pi}}{2} s \sin \theta \left[1 - \mathrm{erf}\,(s \sin \theta)\right] e^{s^2 \sin^2 \theta}}{1 - \sqrt{\pi}\ s \sin \theta \left[1 - \mathrm{erf}\,(s \sin \theta)\right] e^{s^2 \sin^2 \theta}}$$

χ dimensionless group defined by

$$\chi = e^{-s^2 \sin^2 \theta} + \sqrt{\pi}\ s \sin \theta \left[1 + \mathrm{erf}\,(s \sin \theta)\right]$$

χ' dimensionless group defined by

$$\chi' = e^{-s^2 \sin^2 \theta} - \sqrt{\pi}\ s \sin \theta \left[1 - \mathrm{erf}\,(s \sin \theta)\right]$$

$\mathrm{erf}(a)$ error function $\left(\dfrac{2}{\sqrt{\pi}} \displaystyle\int_0^a e^{-x^2}\, dx \right)$, dimensionless

ANALYSIS

The general problem of the calculation of aerodynamic forces and heat transfer to a body in a free-molecule-flow field is amenable to solution by application of the simpler concepts of the kinetic theory of gases. The simplification arises from the assumption that the motions of molecules that strike the body are in no way affected by collisions with molecules that have struck the body and have returned to the main stream of gas. This basic postulate allows the molecular motions of the oncoming stream to be treated as having the classical Maxwellian velocity distribution superimposed on a uniform mass velocity. Hence, the severe complication of dealing with a nonuniform gas is avoided. Of course, this assumption does not imply that returning molecules do not collide with oncoming molecules since collisions do occur, on the average, at a distance from the body equal to one mean free path. However, if this mean free-path length is large compared with the body dimensions, it can be seen from geometrical considerations that the probability is small that the impinging molecules that do collide with returning molecules will strike the body without first having had their original Maxwellian velocity restored by collisions with other impinging molecules. It would seem probable, also, that a high value of mass velocity compared with the random thermal velocity of the gas would favor free-molecule flow because the re-emitted molecules would tend to be swept along with the stream away from the zone of influence of the body.

In general, the mechanism of energy and momentum transfer for free-molecule flow are inseparable. In effect, this means that the drag on a body is affected by the surface temperature of the body. This state of affairs arises because of the fact that a portion of the momentum imparted to the body is due to the emission of molecules from the surface and the velocity of emission depends upon the temperature of the body. This phenomenon will be discussed in detail later.

Because of the assumption that the motions of the oncoming and re-emitted molecules can be treated independently, the computation of the drag on and heat transfer to a cylinder can be broken down into separate parts — the part due to impact by impinging molecules and a part due to re-emission of the molecules from the surface. By the use of this basic principle, it is possible to calculate the drag and heat-transfer characteristics of a transverse cylinder in a free-molecule-flow field.

Heat Transfer to a Transverse Cylinder
in a Free-Molecule-Flow Field

The calculation of the heat-transfer or energy-exchange process between the cylinder and the gas is made by using the basic method

described in reference 4. The general equations of reference 4 are
expressed in Cartesian coordinate form and can be summarized as follows:

The translational molecular energy incident upon the front side of
an elemental plane area dA inclined at an angle θ with respect to the
stream mass velocity U is, for a monatomic gas,

$$dE_t = n \left(\frac{mU^2}{2} + \psi kT \right) dA \tag{1}$$

where n, the number of molecules striking unit surface area per second,
is given by

$$n = \frac{Nv_m}{2\sqrt{\pi}} \chi \tag{2}$$

For the rear side of the elemental area, similar expressions apply.

$$dE_t' = n' \left(\frac{mU^2}{2} + \psi' kT \right) dA \tag{3}$$

$$n' = \frac{Nv_m}{2\sqrt{\pi}} \chi' \tag{4}$$

The total molecular energy incident upon the front and rear sides
of dA is, for a monatomic gas, given by equations (1) and (3), respec-
tively, since only translational energies are involved. However, for a
diatomic gas, the expression for the incident energy contains an additional
term due to the rotational component of the molecular internal energy, and
this component must be added to the translational component. The rotat-
ional energy per molecule of a gas composed of rigid dumbbell molecules is

$$E_R = kT \tag{5}$$

Then, the total incident molecular energy on the front side of dA
is, for a diatomic gas, given by the following expression:

$$dE_i = dE_t + nE_R dA = n \left[\frac{mU^2}{2} + (\psi+1)\ kT \right] dA \tag{6}$$

and, for the rear side of dA,

$$dE_i' = dE_t' + n'E_R dA = n' \left[\frac{mU^2}{2} + (\psi'+1)\ kT \right] dA \tag{7}$$

The method of calculation of the energy transported from the elemental
area by re-emitted molecules is shown in appendix A. The result derived

therein can be applied to the calculation of the energy transport by a monatomic gas from the front side of the area by combining equations (A1) and (A12) to yield

$$dE_r = dE_t(1-\alpha) + 2\alpha n k T_c\ dA \qquad (8)$$

and, for the energy transport by a diatomic gas, as

$$dE_r = (dE_t + nkT\ dA)(1-\alpha) + 3\alpha n k T_c dA \qquad (9)$$

Parallel equations can be written for the rear side of the area, dA.

The net radiant energy exchange is (assuming gray—body radiation)

$$\epsilon\sigma\left(T_c^4 - T_t^4\right)\ dA \qquad (10)$$

where T_t is the effective temperature of the surroundings to which the area dA is radiating. This expression implies that the body of which dA is a part is small in comparison with the surrounding volume.

The problem now becomes one of applying the foregoing equations, which were derived for a plane area placed at an arbitrary angle with respect to the stream, to a specific body — in this case a cylinder with axis perpendicular to the stream velocity. For a cylinder of length L, the elemental area may be written as

$$dA = rLd\theta \qquad (11)$$

Then, if internal energy input to the cylinder per unit area is denoted as Q (in the usual experimental arrangement this would be electrical energy), an equation can be written which expresses an energy balance on the cylinder. For a monatomic gas, the energy—balance equation is

$$2\alpha rL\left[\int_0^{\pi/2} n\left(\frac{mU^2}{2} + \psi kT\right)\ d\theta + \int_0^{\pi/2} n'\left(\frac{mU^2}{2} + \psi' kT\right)\ d\theta\right] -$$

$$4\alpha rLkT_c\left(\int_0^{\pi/2} nd\theta + \int_0^{\pi/2} n'd\theta\right) + 2\pi rL\left[Q - \epsilon\sigma\left(T_c^4 - T_t^4\right)\right] = 0$$

$$(12)$$

For a diatomic gas, a similar equation applies

$$2\alpha r L \left\{ \int_0^{\pi/2} n \left[\frac{mU^2}{2} + (\psi+1)kT \right] d\theta + \int_0^{\pi/2} n' \left[\frac{mU^2}{2} + (\psi'+1)kT \right] d\theta \right\} -$$

$$6\alpha r L k T_c \left(\int_0^{\pi/2} n d\theta + \int_0^{\pi/2} n' d\theta \right) + 2\pi r L \left[Q - \epsilon\sigma \left(T_c^4 - T_t^4 \right) \right] = 0 \qquad (13)$$

The reduction of the integrals appearing in equations (12) and (13) is a straightforward but lengthy procedure. The methods used to evaluate these integrals are given in appendix B. The final results are written here, for a monatomic gas, as

$$2 \frac{T_c}{T} (Z_1+Z_2) - \left[Z_1(s^2+2) + Z_2\left(s^2+ \frac{5}{2}\right) \right] + \frac{2\pi^{3/2}}{p v_m \alpha} \left[\epsilon\sigma(T_c^4 - T_t^4) - Q \right] = 0 \qquad (14)$$

and, for a diatomic gas, as

$$3 \frac{T_c}{T} (Z_1+Z_2) - \left[Z_1(s^2+3) + Z_2\left(s^2+ \frac{7}{2}\right) \right] + \frac{2\pi^{3/2}}{p v_m \alpha} \left[\epsilon\sigma(T_c^4 - T_t^4) - Q \right] = 0 \qquad (15)$$

In order to facilitate computation, values of the dimensionless groups,

$$f(s)= Z_1(s^2+3)+Z_2\left(s^2+ \frac{7}{2}\right), \quad g(s)= 3(Z_1+Z_2), \quad f^o(s)= Z_1(s^2+2)+Z_2\left(s^2+ \frac{5}{2}\right),$$

and $g^o(s) = 2(Z_1+Z_2)$, appearing in equations (14) and (15), are tabulated in the table of appendix B.

Equations (14) and (15) then completely describe energy transfer occurring between a transverse cylinder and its surroundings in terms of the cylinder temperature, static gas temperature and pressure, molecular-speed ratio, accommodation coefficient, the effective temperature of the surroundings to which the cylinder is emitting radiation, the emissivity of the cylinder surface, and the internal energy input to the cylinder. The equations are subject to the following restrictions:

1. The surface temperature of the cylinder is assumed to be constant, circumferentially.

2. The cylinder receives and emits radiant energy as a gray body; that is, the emissivity is independent of wave length. Also, the cylinder is assumed to be small compared to the surrounding volume.

3. The internal energy of the gas stream in which the cylinder is located has the value $(3/2)kT$ for a monatomic gas and $(5/2)kT$ for a diatomic gas.

Drag on a Transverse Cylinder in a Free—Molecule—Flow Field

The general problem of aerodynamic forces acting on bodies in free—molecule flow has been treated by several authors (references 1, 2, and 3). The basic method of calculation was identical in each case. The method consists of the assumption of a gas with a Maxwellian velocity distribution superimposed upon an arbitrary mass velocity. The number of molecules having specified velocities that impinge upon an elemental area inclined at an arbitrary angle to the stream mass velocity is computed and, from this calculation, the force due to the transmitted momentum is obtained. To this momentum due to molecular impingement, however, must be added the momentum imparted to the surface by molecules emitted from the surface. The magnitude and direction of the force imparted by emitted molecules depends, among other things, on the type of emission that is assumed to occur. A condensed discussion of the several possible types of surface emission can be found in reference 4. An extensive treatment of the subject is given in reference 7.

In order to determine the total aerodynamic force on a body of arbitrary shape, the differential momentum imparted to an element of the body surface is computed, as outlined in the preceding paragraph, and the total momentum obtained by integration over the body surface. Also, since the impinging and re—emitted momenta can be added linearly, the resulting total momentum can be calculated for any desired type of re—emission.

In this paper, completely diffuse scattering of the incident molecular stream from an insulated surface is assumed. By this assumption it is meant that (a) the molecules that are scattered from the surface are emitted with a Maxwellian distribution of speed, (b) the direction of molecular emission from the surface is controlled by the Knudsen cosine law (cf., references 7 and 8), (c) the body temperature is assumed to be uniform over the surface, and further (d) that conservation of number of molecules is maintained for each element of the body surface. These assumptions seem to be in accord with physical fact, as discussed in reference 6.

The specific problem of the aerodynamic drag on a transverse cylinder has been treated in references 1 and 3. The reason for repetition of the calculation here is that the results have been obtained in a compact closed form which is amenable to easy calculation and, further, that a solution for the re—emission drag is obtained which involves measurable physical quantities. Appendixes A and C contain the details of the calculations and only the final results are presented here. The results of the computations are as follows: The total drag acting on an insulated transverse circular cylinder of radius r and length L is given by

$$D = \frac{\rho U^2}{2} (2rL)(C_{D_i} + C_{D_r}) \tag{16}$$

where C_{D_i} and C_{D_r} are the drag coefficients associated with impinging and re-emitted momenta. The value of C_{D_i} is shown in appendix C to have the value

$$C_{D_i} = \frac{\pi^{1/2}e^{-s^2/2}}{s} \left\{ I_0(s^2/2) + \left(\frac{1+2s^2}{2}\right) \left[I_0(s^2/2) + I_1(s^2/2) \right] \right\} \quad (17)$$

and the value of C_{D_r} for an insulated cylinder is shown in appendix A to be, for a monatomic gas,

$$C_{D_r} = \frac{\pi^{3/2}}{4s} \sqrt{\frac{Z_1(s^2+2) + Z_2\left(s^2+\frac{5}{2}\right)}{2(Z_1+Z_2)}} \quad (18)$$

and, for a diatomic gas,

$$C_{D_r} = \frac{\pi^{3/2}}{4s} \sqrt{\frac{Z_1(s^2+3) + Z_2\left(s^2+\frac{7}{2}\right)}{3(Z_1+Z_2)}} \quad (19)$$

APPARATUS AND TEST METHODS

The Wind Tunnel

The Ames low-density wind tunnel, in which the present tests were conducted, is an open-jet nonreturn-type tunnel. A sketch showing the major components of the wind tunnel is shown in figure 1. The test gas, from a bottled source, is throttled into a settling chamber and then passes through an axially symmetric nozzle which discharges a free jet into an 18-inch cubical test chamber. The test chamber is connected through a surge chamber to four booster-type oil-diffusion pumps which continuously evacuate the system. The diffusion pumps are connected in parallel and are backed by a mechanical vacuum pump which discharges to the atmosphere. Valves are provided at the inlet to each diffusion pump in order to allow the pumping system to be isolated when the test chamber is opened to the atmosphere.

A traversing mechanism is installed in the test chamber which permits three degrees of motion relative to the gas stream. The mechanism is used to position models and instrumentation in the desired location within the gas stream.

The nozzles used in the tests were axially symmetric with an outlet diameter of 2 inches and were machined from clear plastic. The nozzle contours were determined by the method outlined in reference 9. No boundary-layer correction was applied to the nozzle contours.

After the system was evacuated, the flow rate of the test gas into the settling chamber was adjusted until the stagnation pressure, as measured by a McLeod gage, reached the desired value.

The static pressure in the test chamber was read on another McLeod gage and, if the resulting pressure ratio was that required to establish flow at the particular Mach number desired for the run, the tunnel was considered ready for tests. In order to match tunnel conditions of static pressure and pressure ratio with those that existed at an earlier time, it was sometimes necessary to alter the amount of throttling at the pump inlets due to a slight variation of pumping speed from day to day.

The pressure level in the tunnel was varied by increasing or decreasing the flow of the test gas into the system. The static and stagnation pressures were again checked to determine if sufficient pressure ratio was available to establish flow at the desired Mach number. This procedure was somewhat complicated by the fact that at the lower pressure levels the boundary layer in the nozzle would tend to thicken, thus causing a decrease in the Mach number compared with that obtained at the higher pressure levels.

The wind tunnel could be operated through a range of test-section pressures of from 20 to 135 microns of mercury for a given nozzle and over a range of Mach numbers from 0.5 to 2.75 by using several nozzles.

Instrumentation and the Test Model

The static pressures which existed in the wind tunnel were, in general, too low to be measured with a conventional manometer or Bourdon-type pressure gage; therefore, two types of gages widely used in high-vacuum work were utilized, namely, the McLeod and Pirani gages. For a complete description of these gages the reader is referred to any standard text on high-vacuum technique (e.g., reference 10); however, some of the special features of the gages used will be described.

The McLeod gage used as a primary standard in these tests had an initial volume of 146 milliliters connected to a closed tube of 1.95-millimeter diameter. This arrangement gave a scale length of 51.4 centimeters for a pressure range of 0 to 3000 microns. (For the sake of brevity, the term micron is used throughout as a unit of pressure rather than the term microns of mercury.) The diameter of the closed tube was measured by the mercury pellet method to within ±0.01 millimeter and the difference in height of the mercury columns could be read to the nearest 0.1 millimeter by use of a micrometer scale. At a pressure of 100 microns, this gage could be read to within 1 percent with ease.

The gage was connected to the test chamber with an 18-millimeter-diameter glass tube to insure a short time lag between equalization of the system and the gage pressures. A dry-ice and acetone cold trap was provided between the gage and the test chamber to prevent condensable vapors from reaching the gage.

In general, it is difficult to obtain a completely independent method of checking the accuracy of pressure measurements made with a McLeod gage for pressures below about 1 millimeter of mercury. Above 1 millimeter of mercury a U-tube manometer, filled with a very low-vapor-pressure oil and having a high-vacuum system (of the order of 10^{-5} mm of Hg) connected to one leg, may be used. The McLeod gage used in the tests was checked in this manner and the agreement between the oil manometer and the McLeod gage was within ±3 percent.

An indication of the accuracy of the McLeod gage used in the tests in the pressure range below 200 microns was obtained by comparing the pressures indicated by the test McLeod gage with those obtained with a laboratory-type McLeod gage having a range of 0 to 200 microns, which has been calibrated against a laboratory standard McLeod gage at the manufacturer's plant. The agreement between the test gage and the laboratory-type gage was within ±3 percent at a pressure of 100 microns.

The Pirani gage used in the tests consisted of an open glass tube, which contained a heated filament. The gas pressure in the tube determined the temperature and thus the resistance of the filament. A temperature-compensating tube of identical construction was sealed off at a very low pressure. The measuring and compensating tube filaments formed two legs of a Wheatstone bridge; and the unbalance of the Wheatstone bridge circuit, as indicated by a self-balancing potentiometer, was a measure of the pressure in the open leg of the gage. The Pirani gage was calibrated against the 0- to 3000-micron-range McLeod gage as a standard.

A drift of the calibration of the Pirani gage with time was noted and for this reason the Pirani gage was calibrated before and after every test run. A typical calibration curve is shown in figure 2.

Examination of figure 2 reveals that the sensitivity of the Pirani gage used was nearly constant from a pressure of 10 microns to a pressure of 80 microns. Above about 200 microns this Pirani gage becomes too insensitive to be usable as a pressure-measuring instrument.

Whenever a pressure-measuring device is connected to a vacuum system by a tube or small orifice, two troublesome effects are present — time lag and gassing. The time lag of the pressure gage is due to the fact that, as the pressure in the main part of the system is changed, a volume of gas must flow out of or into the pressure gage and its connecting tubing. At the low pressures encountered during the tests, this time lag may be of the order of hours if the gage volume and connecting tubing

are not properly proportioned. Gassing, that is, gas being given up or
adsorbed by the surface of the pressure gage and its connecting tubing,
has the effect of causing the pressure gage to indicate a different
pressure than that which exists in the main part of the system. Out-
gassing effects can be reduced materially by proper cleaning of the
surface and by heating the surface under a vacuum to drive off water
vapor and other materials which cling to ordinary surfaces.

Schaaf, Mann, and Cyr (references 11 and 12) have investigated this
problem in considerable detail, and show that, if the assumption is made
that gassing is a function of surface area only, there exists an optimum
geometry of gage volume and connecting tubing which will result in mini-
mum time lags. References 11 and 12 were used as guides in the design
of the impact and static-pressure-measuring devices which were used in
the tunnel calibration tests, and, in addition, the time lag of these
pressure-measuring systems was measured.

The impact pressures encountered during the wind-tunnel-calibration
tests were too high to be measured with a Pirani gage and, because of the
difficulty of obtaining a suitable flexible tube which would have a small
time lag, the McLeod gage could not be used. These impact pressures,
therefore, were measured with a glass U-tube manometer filled with a
low-vapor-pressure oil. The manometer was located inside the test cham-
ber with one leg of the manometer open and the other end fastened with a
glass connection to a 1/8-inch-diameter spherical-head impact tube.
Figure 3 shows a diagrammatic sketch of this arrangement. The difference
in oil level between the two legs, as read by a coordinate-type cathetom-
eter located outside the tunnel, was the difference between the test-
chamber static pressure and the impact pressure. The test-chamber static
pressure was measured by the 0- to 3000-micron McLeod gage described
earlier.

The time lag of the system shown in figure 3 was measured by setting
the pressure in the test chamber at approximately 3 millimeters of
mercury and then evacuating the chamber to approximately 10 microns as
quickly as possible. The time required for the oil level in the two
legs to equalize was approximately 15 seconds. This indicates a very
short time lag for the practical case as the rate of pressure change
encountered in the wind-tunnel calibration was small compared to that
measured during the time-lag test. The procedure used in the wind-
tunnel-calibration tests was to continue to take readings of the oil
level until steady state was established.

The static pressure of the gas stream from the nozzle was measured
with a 0.10-inch-diameter ogival probe connected directly to a Pirani
gage as shown in figure 4. Three 0.0225-inch-diameter holes spaced 120°
apart were located at a point on the ogive where the pressure is equal
to free-stream pressure as calculated by the method given in reference
13. The position along the probe where the surface pressure is equal

to free—stream pressure varies somewhat with Mach number; however, this variation is not large and static pressures measured by this probe agreed with pressures measured with a 4°cone.

No boundary—layer correction was applied to the ogive, or cone contour; consequently, it is possible that some error in the measurement of static pressure existed. Figure 5 shows the main dimensions of the static—pressure probe used.

In order that the Pirani gage shown in figure 4 could be calibrated against the McLeod gage, which was connected to the test chamber, a 4—millimeter—bore stopcock was glass—welded to the Pirani gage to allow calibration with a relatively large opening and attendant short time lag. As the stream static pressures were measured with the stopcock closed, the following tests were conducted to measure the order of magnitude of the time lag of the system. The test chamber was pressurized to 165 microns and suddenly evacuated to approximately 5 microns. The rate of pressure change as measured by the Pirani gage with the stopcock open and with the stopcock closed is shown in figure 6. The procedure was repeated with a rising pressure and the results are also shown in figure 6.

It can be seen from figure 6 that the two curves, representing the runs with the stopcock open and closed, are essentially congruent after 70 seconds for decreasing pressure and after 50 seconds for the increasing pressure runs. With the stopcock open, the time lag of the Pirani gage should be very small (references 11 and 12) and the curve of pressure as a function of time includes the time required for the pumping equipment to evacuate the test chamber, the time lag in the self—balancing potentiometer, and the thermal lag in the Pirani filaments. The curve of pressure as a function of time for the stopcock closed includes all these factors plus the additional time lag imposed by the small holes in the static probe. The pressure variation during the time—lag tests was much more severe than any encountered during the static survey tests; therefore, it can be concluded that, by waiting for at least 2 minutes before recording data, all errors due to time lag would be eliminated.

The test model.— The model tested was a 0.0031—inch—diameter right—circular cylinder fabricated from iron and constantan wires and had an exposed length of 15/32 inch. The iron and constantan wires were electrically butt—welded together to form a thermocouple junction. Figure 7 shows a microphotograph of the model. It can be seen that the welding operation did not appreciably alter the shape of the model. The butt—welded junction was located in the center of the model and a 0.0031—inch iron wire was silver soldered to the constantan side of the model at a distance of 5/16 inch from the center junction. A 0.0031—inch—diameter constantan wire was similarly fastened to the iron side of the model. These two auxiliary thermocouple junctions were used to measure the temperature at the ends of the model.

The entire model was covered with fine-grain soot obtained from an acetylene flame in order that the emissivity would be constant over the total model length and so that an established value of emissivity of 0.95 could be used to evaluate the heat loss by radiation.

Thermocouple voltages from the center and end thermocouples were read on a null-type laboratory potentiometer having a least count of 0.01 millivolt.

The drag balance.- A specially constructed microbalance shown in figures 8(a) and 8(b) was used to measure the drag of the model tested. The balance consisted of a beam mounted upon an agate knife-edge which rested in a steel V-block, as shown diagrammatically in figure 9. The model was mounted between two arms extending down from either side of the beam. Electrical leads were transferred from the moving beam to the balance frame through mercury pools.

A drag force on the model caused an unbalance of the beam which was counteracted by a magnetic-restoring force produced by an armature located in a magnetic field produced by an alternating-current coil. An optical lever approximately 2 feet long was used to determine the zero position of the balance.

The magnitude of the drag force in terms of magnetizing current was determined by hanging known weights on a lever arm attached to the balance beam and measuring the current necessary to restore the balance to zero position. Figure 10 shows a typical calibration of the drag balance.

The model was mounted between the extension arms of the drag balance and was shielded over all but the center 15/32 inch, as shown in figures 8(a) and 8(b). A check was made on the effectiveness of the shielding on the supporting members. A small shield was mounted to the center main shield (extension arms) covering the center portion of the model (normally exposed). The completely shielded model was then placed in the gas stream. No drag forces were detected.

It was found that the balance exhibited an erratic calibration shift from day to day, which necessitated calibration of the balance before and after each drag determination.

Calibration of the Wind Tunnel

The purpose of the calibration of the wind tunnel was to determine the Mach number and static-pressure distributions of the stream in the plane at which the model was located - 1/4 inch downstream of the exit plane of the various nozzles used.

The method used was to survey the stream with the impact- and static-pressure probes described earlier. These impact- and static-pressure probes, together with their pressure-measuring gages, were

mounted 2 inches apart upon a common support from the traversing mecha-
nism and readings were taken at 1/16-inch intervals from the center to
the edge of the stream. This method of mounting allowed both the impact
and static pressures to be measured during the course of one run, thus
obviating the necessity of matching tunnel conditions on separate runs.

Table I lists the nozzles tested, their design Mach number, and the
tunnel conditions for which the surveys were made.

The static pressure varied across the stream issuing from each of
the nozzles tested. For most of the nozzles, the pressure was somewhat
higher near the center portion of the stream than was the pressure of
the quiescent gas in the test chamber. Certain of these nozzles,
however, did not show this general trend. In these nozzles the pressure
first decreased, then increased, as the probe was moved from the nozzle
wall to the center of the stream. Figures 11 and 12 show this effect.
In general, the static-pressure variation across the stream was not
large. The average change over the center 1/2 inch of the stream
amounted to 2 percent, while the maximum deviation was only 5 percent.

The impact-pressure surveys of all the nozzles had one common
characteristic; that is, the impact pressure increased from a minimum
value at the edge of the nozzle wall to a maximum value near the center
of the stream. The area of the stream which had a constant, or nearly
constant, impact pressure varied somewhat from nozzle to nozzle, and
also to some extent with pressure level. The average variation of impact
pressure over the center 1/2 inch of the stream for all nozzles tested
was 7 percent with a maximum variation in some cases of 14 percent.
Figures 11 and 12 show the variation of impact pressure across the stream
for one nozzle using two gases, nitrogen and helium.

The Mach number of a gas stream can be computed from measured values
of the stagnation and static pressure of the stream, provided that the
flow is isentropic between the points of pressure measurement. However,
if the static and impact pressures are measured at the same point in the
stream, no assumption regarding the nature of the flow need be made in
order to compute the local stream Mach number. For an inviscid flow,
the Mach number can be calculated from Rayleigh's equation, the use of
which involves the assumption of a normal shock wave ahead of the impact-
pressure tube and isentropic compression of the gas in the subsonic flow
behind the shock wave to the stagnation point on the impact-pressure tube.
In a low-density flow, however, viscous effects are present in the flow
about a stagnation region, thus invalidating the assumption of isentropic
compression behind the normal shock wave. Chambré (reference 14) computed
the viscous correction to be applied to spherical-head impact tubes in a
low-density flow, and figure 13 shows the Mach number distribution of
nozzle 1 as computed by the Rayleigh equation (inviscid) and as
computed by Chambré's equation. The Mach number calculated from the
stagnation and local static pressures were, in all cases, higher than
those computed using local values of impact and static pressure, thus

indicating that the flow through the nozzle was nonisentropic due to viscous effects. Chambré's equation was used to compute Mach number from measured static and impact pressures for the tests described herein.

The variation of impact and static pressure across the stream resulted in a stream in which the Mach number was not constant. Figures 13 and 14 show this effect and are generally representative of all nozzles tested. If only the center 1/2 inch of the nozzles is considered, the average variation in Mach number amounted to 5 percent; however, at certain pressure levels in some of the nozzles the variation was as much as 14 percent.

In order to determine if shock waves were present in the center 1/2 inch of the gas stream, the nitrogen-glow-discharge technique of flow visualization was used to examine the flow qualitatively. This technique was originally described in reference 15. The method used to generate the glow discharge was to pass the test gas through a screen which was connected to a pulsed direct-current power supply. The screen was located at the entrance plane to the nozzle and was pulsed to a negative peak potential of 1000 volts. The pulsation frequency was 1000 cycles per second.

Figure 15 shows the gas stream from nozzle 1 at a static pressure of 114 microns. A 5° half-angle wedge was placed in the stream to generate a relatively weak shock wave which could be used as a yardstick to evaluate the strength of the nozzle shocks, if present. No shock waves were observed in the gas stream at this pressure level if the wedge was removed. As the static-pressure level was lowered, the shock wave from the wedge became too indistinct to be photographed. Observation of the nitrogen glow did not indicate the presence of strong shock waves in the nozzles.

Drag and Heat-Transfer Tests

The test procedure used in the drag and heat-transfer experiments was to calibrate the drag balance with the tunnel shut down and then to set tunnel conditions corresponding to those obtained during tunnel-calibration tests by matching the stagnation and test chamber static pressures. As extremely close control over tunnel conditions was difficult to attain, the pressure level during certain test runs varied approximately 5 percent from those obtained during the tunnel-calibration tests. Examination of the results of the tunnel-calibration tests showed that Mach number variation is small for small changes in the pressure level; therefore, the Mach number obtained during nozzle-calibration tests was applied to the heat-transfer and drag tests without correction. The Mach number used in plotting the data (which was converted numerically to molecular-speed ratio by means of the relation $s = M\sqrt{\gamma/2}$) was the average value obtained from a graphical integration of the Mach number distribution across the center 15/32 inch of the stream.

After stable operating conditions had been attained, the drag force, model temperatures, and other pertinent data were recorded. Table II lists the recorded data. It will be noted that, in the column listing the recorded drag force, two values occur on some of the runs. The different values were due to separate drag measurements during the course of one run or resulted from small shifts in the calibration of the drag balance as determined before and after each run. In the figures which are later presented, showing drag coefficients, the points correspond to those calculated using the average of the two values listed in table II.

To determine if the model surface conditions were changing with time, the model drag and temperature were measured at 1/2-hour intervals over a period of 6 hours for one particular test condition. Figures 16 and 17 show the results of these tests and it can be seen that the drag coefficient and temperature ratio remained essentially constant, thus indicating that the accommodation coefficient and tunnel conditions were constant over this period of time.

The reproducibility of the data was checked by repeating the above-described run on separate days. The reproducibility was found to be within the accuracy of the drag and temperature measurements described above.

RESULTS AND DISCUSSION

A Discussion of the Assumptions and Results
of the Theoretical Analysis

An examination of the heat-transfer equations (14) and (15) for a monatomic and a diatomic gas, respectively, reveals several interesting features. If an adiabatic case is considered; that is, if both internal-energy input to the cylinder and radiant-energy exchange are considered absent, it can be seen that the ratio of cylinder temperature to free-stream static temperature is a unique function of the molecular-speed ratio. The values of the temperature ratio computed from equations (14) and (15) are shown in figure 18. For comparison, curves of the temperature ratio for continuum flow are also shown. These latter curves were computed for the case where the total stream energy is recovered — in other words, the temperature recovery factor was considered to be unity. Several remarkable conclusions can be drawn from an examination of this figure. It can be seen that an insulated cylinder in a free-molecule-flow field will attain a higher temperature at a given value of molecular-speed ratio (or Mach number) than will be obtained in a continuum flow field. Since the continuum curves also represent the temperature ratio of a gas that has been accelerated adiabatically from rest to any value of molecular speed ratio, it may be inferred that an insulated cylinder located in a low-density wind tunnel under free-molecule-flow conditions

will attain a temperature which exceeds the total temperature of the gas stream. This result, of course, is in direct contrast to the corresponding phenomenon which occurs under continuum flow conditions where an insulated body can have, at most, a temperature equal to the stream stagnation temperature and normally does not even attain this temperature due to outward heat flow in the boundary layer. The anomaly can be explained, however, by a consideration of the magnitudes of the incident and re-emitted molecular energy. The incident molecular energy is computed using the total velocity resulting from combination of the stream mass velocity and the random thermal velocities. When the total-velocity term is squared there results a cross-product term, $2UV$. This cross-product term effectively increases the apparent internal energy of the gas from the continuum value of $(3/2)kT$ per molecule to a value from $2kT$ to $(5/2)kT$, depending upon the speed and orientation of the body. The apparent internal energy becomes $(5/2)kT$ for high speeds and body angles of attack greater than zero. This is just equal to the interal plus potential energy per molecule of a cube of continuum gas. Therefore, the energy incident on the body in free-molecule flow becomes equal to that of a continuum for large values of the molecular-speed ratio for surfaces inclined at angles of attack greater than zero. The molecular energy which is re-emitted from the surface is assumed to be equal to the energy of a Maxwellian stream issuing effusively from a gas, in equilibrium at some yet unspecified temperature, into a perfect vacuum. For the case of an insulated body the temperature of this gas is that of the body. The energy of the re-emitted stream calculated in this manner is given by equation (A12) to be equal to $2kT_w$ per molecule. The corresponding energy for a continuum gas at the same temperature is $(5/2)kT_w$ per molecule if both thermal and potential energies are considered. Because of the net energy deficiency of the re-emitted effusive stream for a given wall temperature, a body in free-molecule flow will attain a temperature higher than that attained in a continuum flow.

It is seen from figure 18 that, theoretically, a higher cylinder temperature is predicted for the case of a monatomic gas than for a diatomic gas. The explanation lies in the additional energy which the diatomic gas is able to remove from the cylinder by virtue of the internal energy component due to molecular rotation. Of course, the impinging diatomic gas transmits more energy to the cylinder due to the rotational energy component; however, the rotational component is a smaller fraction of the total impinging energy than of the total re-emitted energy.

An examination of the equations for the drag coefficient of an insulated cylinder (equations (17) and (18)) shows that the total drag coefficient, $C_D = C_{D_i} + C_{D_r}$, is a function only of the molecular-speed ratio. A plot of the total drag coefficient as a function of the molecular-speed ratio for an insulated cylinder is shown in figure 19. It is notable that the drag coefficient approaches infinity as the molecular-speed ratio approaches zero. Hence, if the expression for total drag is written in the conventional drag-coefficient form, it can be shown from

equations (17) and (18) that C_D becomes inversely proportional to the speed ratio as s approaches zero. It is also notable that the drag coefficient approaches a constant value as the speed ratio becomes large. This means, simply, that the effect of the random thermal motions becomes negligible as the speed of the cylinder relative to the gas becomes high.

Heat—Transfer Test Results

The salient point of the analysis concerning heat transfer to a cylinder in a free—molecule field was the prediction that an insulated model would attain a temperature in excess of the tunnel stagnation temperature. This result was observed in all runs. The maximum rise of the model center—point temperature above the tunnel stagnation temperature was 65° F, using nitrogen as the test gas, and 147° F, using helium as the test gas.

The results of the heat—transfer tests are shown in figures 20 and 21 in which the ratio of the cylinder—center temperature to the free—stream static temperature is plotted as a function of the molecular—speed ratio for the nitrogen and helium runs, respectively. The stream—static temperature was computed from the adiabatic relationship, using the measured value of Mach number (or molecular—speed ratio) corresponding to the nozzle pressure ratio as determined from the nozzle—calibration tests. The temperature ratio curve for continuum flow assuming a temperature—recovery factor of unity is shown for comparison. It will be noted that in all cases the temperature ratio exceeded the maximum which could be attained under continuum flow conditions. It can be seen that, in general, the test points indicate that the cylinder did not attain the full temperature rise that was predicted by the free—molecule analysis. This result may be ascribed to heat losses occurring from radiation and from conduction along the wire to the end supports. The fact that a large temperature gradient existed along the length of the wire due to end losses is clearly shown by the cylinder—end temperatures which are listed, together with the cylinder center—point temperature, in table II.

Drag Test Results

The measured drag force on the cylinder was reduced to conventional dimensionless drag—coefficient form by means of the equation

$$C_D = \frac{D}{\gamma LrpM^2} = \frac{D}{2Lrps^2} \tag{20}$$

The data points obtained from equation (20) are shown in figure 22. For comparison, the theoretical curves of drag coefficient as a function of molecular—speed ratio for an insulated cylinder, taken from figure 19,

are shown as a solid line. It can be seen that agreement between theory
and experiment is good considering the limitations of the theory and the
difficulties attendant with the measurement of drag forces from 1 to 20
milligrams. The experimental values for the drag coefficient tend to
fall below the theoretical values at molecular-speed ratios above about
1.0 and to be higher than the theoretical values at speed ratios below
1.0. The former characteristic may be due to a tendency toward specular
reflection at the higher speed ratios while the latter characteristic, at
subsonic values of speed ratio, may have been caused by interference with
the flow caused by the shields at the ends of the model.

The major premise of the existence of free-molecule flow was borne
out by several factors in addition to the good agreement between the
calculated and experimental values of drag coefficient. One of the
basic assumptions of the drag analysis is that the drag coefficients
are independent of Reynolds number or Knudsen number. In contrast, the
continuum and slip-flow regimes are characterized by the dependence of
drag coefficients both upon Reynolds number and Mach number (cf.,
reference 16). Although it was not experimentally possible to vary the
Knudsen number independently of the speed ratio for one test gas, the
use of both nitrogen and helium gave overlapping values of speed ratio
with an approximate 2:1 variation of Knudsen number. The variation of
Knudsen number covered by the tests with molecular-speed ratio is shown
in figure 23. No trend is noticeable in the drag coefficients obtained
in each case; consequently, it can be concluded that free-molecule flow
existed.

A comparison between measured drag coefficient and the drag coeffi-
cient calculated by methods as given by Lamb (reference 17) illustrates
the inapplicability of continuum theory in the free-molecule regime. A
sample calculation made by Lamb's continuum method for conditions of
molecular speed ratio equal to 0.5 and a Knudsen number of 185 (based on
cylinder radius) gave a drag coefficient of 390. The corresponding
experimental value was 14.6.

CONCLUSIONS

The following conclusions may be drawn from a comparison of the
test results with free-molecule-flow theory shown in this report:

1. The salient point of the heat-transfer analysis, which was the
prediction that an insulated cylinder would attain a temperature higher
than the stagnation temperature of the stream, was confirmed by the
test results.

2. Drag coefficients, calculated from free-molecule-flow theory,
agreed well with the measured drag coefficients. As predicted

theoretically, the measured drag coefficients were independent of the
Reynolds and Knudsen numbers and depended primarily upon the molecular-
speed ratio.

Ames Aeronautical Laboratory,
    National Advisory Committee for Aeronautics,
        Moffett Field, Calif., Sept. 12, 1950.

APPENDIX A

THE MOMENTUM AND ENERGY EXCHANGE PROCESSES ACCOMPANYING
MOLECULAR EMISSION FROM A SURFACE

For the case of diffuse scattering of a stream of molecules from a surface, all directional history of the impinging stream is erased upon impact with the surface. The impinging stream is assumed to be scattered in a random manner which will be described in detail later. The energy and momentum carried by the scattered stream depends upon the velocity of emission which can be related to the energy (or temperature) level that the stream has. The effective temperature or energy of the scattered stream depends upon the efficiency of the energy-exchange process that occurs between the solid surface and the impinging stream. This efficiency can be described by introduction of the accommodation coefficient which is defined as

$$\alpha = \frac{E_i - E_r}{E_i - E_w} \tag{A1}$$

where the symbols have the following definitions:

E_i rate of incident molecular energy

E_r rate of re-emitted molecular energy

E_w rate of re-emitted molecular energy that would be carried by the scattered stream if it were a stream issuing from a gas in equilibrium at the surface temperature, T_w

It is assumed that the emitted stream has a Maxwellian distribution of speed corresponding to a gas in equilibrium at an unspecified temperature, T_r. This fictitious gas has, also, an unspecified number of molecules per unit volume, N_r. Now, as shown in reference 8, page 62, the number of molecules scattered from unit surface area per second that have speeds in the range dv and that are moving in a direction that makes an angle lying in the range $d\Omega$ with the normal to the surface is given by

$$dn_r = 2\pi N_r A_r v^3 e^{-\beta_r^2 v^2} \sin \Omega \cos \Omega \, dv \, d\Omega \tag{A2}$$

Then, the normal component of force imparted to the surface by this group of molecules is

$$dG_r = 2\pi N_r A_r m v^4 e^{-\beta_r^2 v^2} \sin \Omega \cos^2 \Omega \, dv \, d\Omega \, dA \tag{A3}$$

and the translational energy carried by this group is

$$dE_r = \pi N_r A_r m v^5 e^{-\beta_r^2 v^2} \sin \Omega \cos \Omega \, dv \, d\Omega \, dA \qquad (A4)$$

By integration of these expressions with respect to Ω and v, the following values are obtained for the total momentum and energy carried by the scattered stream from dA:

$$dG_r = 2\pi N_r A_r m \, dA \int_0^\infty v^4 e^{-\beta_r^2 v^2} \, dv \int_0^{\pi/2} \sin \Omega \cos^2 \Omega \, d\Omega = \frac{N_r m}{4 \beta_r^2} \, dA$$

$$\qquad (A5)$$

$$dE_r = \pi N_r A_r m \, dA \int_0^\infty v^5 e^{-\beta_r^2 v^2} \, dv \int_0^{\pi/2} \sin \Omega \cos \Omega \, d\Omega = \frac{N_r m}{2 \sqrt{\pi} \beta_r^3} \, dA$$

$$\qquad (A6)$$

In order to obtain a value for N_r in terms of known variables, the number of molecules scattered from the surface is equated to the number of molecules striking the surface. The number of molecules per second scattered from unit area is

$$n_r = 2\pi N_r A_r \int_0^\infty v^3 e^{-\beta_r^2 v^2} \, dv \int_0^{\pi/2} \sin \Omega \cos \Omega \, d\Omega = \frac{N_r}{2 \sqrt{\pi} \beta_r} \qquad (A7)$$

and the number of molecules striking unit area per second is shown in reference 4 to be given by

$$n = \frac{NX}{2 \sqrt{\pi} \beta} \qquad (A8)$$

The value of N_r is obtained by equating n_r and n from equations (A7) and (A8), thus,

$$N_r = NX \frac{\beta_r}{\beta} \qquad (A9)$$

By substitution of this value of N_r in the momentum and energy equations, the following is obtained:

$$dG_r = \frac{NmX}{4 \beta \beta_r} \, dA \qquad (A10)$$

$$dE_r = \frac{NmX}{2 \sqrt{\pi} \beta \beta_r^2} \, dA \qquad (A11)$$

An identical analysis yields a value for E_w of

$$dE_w = \frac{NmX \, dA}{2 \sqrt{\pi} \beta \beta_w^2} = 2nkT_w \, dA \qquad (A12)$$

For the case of a diatomic gas where the expression for the re-emission energy per molecule contains an additional term having the value kT_w, which accounts for the rotational energy per molecule, the total re-emission energy has the value $3nkT_w dA$.

Equation (A10) describes the normal re-emission pressure on the front side of a unit inclined area. In order to obtain the net drag force (or pressure) in the direction of the mass velocity U, the pressure on the rear side of the inclined area must be taken into account. The computation of the pressure on the rear side of the area is made in a similar manner to the computation of the pressure on the front side of the area and leads to an expression

$$dG_r' = \frac{NmX'}{4\beta\beta_r} dA \qquad (A13)$$

Then, the net drag force due to re-emission pressure in the direction of U, the mass velocity, is

$$dG_r - dG_r' = \frac{Nm \sin \theta}{4\beta\beta_r} (X - X') dA \qquad (A14)$$

Replacing X and X' by their values, equation (A14) becomes

$$dG_r - dG_r' = \frac{\sqrt{\pi} \, Nms \sin^2 \theta}{2\beta\beta_r} dA \qquad (A15)$$

This expression can be put into drag-coefficient form by use of the following substitutions: $Nm = \rho$, $s/\beta = U$. Equation (A15) then becomes

$$dG_r - dG_r' = \left(\frac{\rho U^2}{2}\right) \frac{\sqrt{\pi} \sin^2 \theta}{s_r} dA \qquad (A16)$$

where s_r is the molecular-speed ratio of the re-emitted stream. Then the re-emission drag coefficient, based on the total area of one side of the plane area, is

$$C_{D_r} = \frac{\sqrt{\pi} \sin^2 \theta}{s_r} \qquad (A17)$$

In order to obtain an expression for s_r which contains measurable or calculable physical quantities it is necessary to write an equation expressing an energy balance on the body in question. For the case of an insulated cylinder, if radiant energy exchange is neglected, only molecular energies are involved and the incident molecular energy can be equated to the re-emitted molecular energy. To write an energy balance equation for a transverse cylinder, it is assumed that the energy balance is maintained for the cylinder as a whole and not for individual elements of the cylinder. This means, essentially, that the cylinder has a uniform

temperature, circumferentially. The total incident molecular energy on the cylinder is, for a monatomic gas,

$$E_i = \frac{2rL\rho}{4\sqrt{\pi}\,\beta^3}\left[\int_0^{\pi/2} \chi\,(s^2+\psi)\,d\theta + \int_0^{\pi/2}\chi'\,(s^2+\psi')\,d\theta\right] \quad \text{(A18)}$$

The total molecular energy emitted from the cylinder surface is

$$E_r = \frac{2rL\rho}{2\sqrt{\pi}\,\beta\beta_r^2}\left(\int_0^{\pi/2}\chi\,d\theta + \int_0^{\pi/2}\chi'\,d\theta\right) \quad \text{(A19)}$$

The values of the integrals are shown in appendix B to be

$$\int_0^{\pi/2}\chi\,d\theta = \frac{Z_1+Z_2}{2} + \sqrt{\pi}\,s$$

$$\int_0^{\pi/2}\chi'\,d\theta = \frac{Z_1+Z_2}{2} - \sqrt{\pi}\,s$$

$$\int_0^{\pi/2}\chi\psi\,d\theta = Z_1 + \frac{5}{4}Z_2 + \frac{5}{2}\sqrt{\pi}\,s$$

$$\int_0^{\pi/2}\chi'\psi'\,d\theta = Z_1 + \frac{5}{4}Z_2 - \frac{5}{2}\sqrt{\pi}\,s$$

When E_i and E_r are equated from equations (A18) and (A19) and the values of the integrals are substituted, the following result is obtained:

$$\frac{1}{4\beta^3}\left[s^2(Z_1+Z_2) + \frac{4Z_1+5Z_2}{2}\right] = \frac{1}{2\beta_r^2\beta}(Z_1+Z_2) \quad \text{(A20)}$$

Therefore,

$$\beta_r = \beta\sqrt{\frac{2(Z_1+Z_2)}{Z_1(s^2+2) + Z_2\left(s^2+\frac{5}{2}\right)}} \quad \text{(A21)}$$

A similar analysis for the case of a diatomic gas where the incident molecular energy is

$$E_i = \frac{rL\rho}{2\sqrt{\pi}\,\beta^3}\left[(s^2+1)\int_0^{\pi/2}\chi\,d\theta + (s^2+1)\int_0^{\pi/2}\chi'\,d\theta + \int_0^{\pi/2}\chi\psi\,d\theta + \int_0^{\pi/2}\chi'\psi'\,d\theta\right]$$
$$\text{(A22)}$$

and the re-emission energy is

$$E_r = \frac{3rL\rho}{2\sqrt{\pi}\,\beta\beta_r^2} \left(\int_0^{\pi/2} \chi d\theta + \int_0^{\pi/2} \chi' d\theta \right) \tag{A23}$$

gives a value of β_r of

$$\beta_r = \beta \sqrt{\frac{3(Z_1+Z_2)}{Z_1(s^2+3)+Z_2\left(s^2 + \frac{7}{2}\right)}} \tag{A24}$$

Now, the total re-emission drag force acting on dA has been shown (cf., equation (A16)) to be

$$dG_r - dG_r' = \left(\frac{\rho U^2}{2}\right) \frac{\sqrt{\pi}\sin^2\theta}{s_r} dA$$

To obtain the total re-emission drag on a cylinder, equation (A16) must be integrated over the cylinder surface, thus,

$$G_r - G_r' = \left(\frac{\rho U^2}{2}\right) (2rL)\frac{\sqrt{\pi}}{s_r} \int_0^{\pi/2} \sin^2\theta\, d\theta = \left(\frac{\rho U^2}{2}\right) (2rL)\frac{\pi^{3/2}}{4s_r} \tag{A25}$$

Then, the re-emission drag coefficient based on the projected cylinder area is

$$C_{D_r} = \frac{\pi^{3/2}}{4s_r} \tag{A26}$$

The final equation for the re-emission drag coefficient for an insulated cylinder in a monatomic gas stream is obtained by using the relation $s_r = U\beta_r$ and taking β_r from equations (A21) and (A24).

$$C_{D_r} = \frac{\pi^{3/2}}{4s} \sqrt{\frac{Z_1(s^2+2)+Z_2\left(s^2+\frac{5}{2}\right)}{2(Z_1+Z_2)}} \tag{A27}$$

and, for an insulated cylinder in a diatomic gas stream, as

$$C_{D_r} = \frac{\pi^{3/2}}{4s}\sqrt{\frac{Z_1(s^2+3)+Z_2\left(s^2+\frac{7}{2}\right)}{3(Z_1+Z_2)}} \qquad (A28)$$

APPENDIX B

HEAT TRANSFER TO A TRANSVERSE CIRCULAR CYLINDER
IN FREE-MOLECULE FLOW

It has been shown (see Analysis) that an energy balance on a cylinder located in a stream of monatomic gas flowing with a velocity U perpendicular to the cylinder axis is expressed by

$$2\alpha rL \left[\int_0^{\pi/2} n \left(\frac{mU^2}{2} + \psi kT \right) d\theta + \int_0^{\pi/2} n' \left(\frac{mU^2}{2} + \psi' kT \right) d\theta \right] -$$

$$4\alpha rLkT_c \left(\int_0^{\pi/2} n d\theta + \int_0^{\pi/2} n' d\theta \right) +$$

$$2\pi rL \left[Q - \epsilon\sigma(T_c^4 - T_t^4) \right] = 0 \tag{B1}$$

Equation (B1) can be simplified by dividing through by $2\pi rL$ and replacing n and n' by their values from equations (2) and (4), thus,

$$\frac{Nv_m\alpha}{4\pi^{3/2}} (mU^2 - 4kT_c) \left(\int_0^{\pi/2} \chi d\theta + \int_0^{\pi/2} \chi' d\theta \right) +$$

$$\frac{\alpha kTNv_m}{2\pi^{3/2}} \left(\int_0^{\pi/2} \chi\psi d\theta + \int_0^{\pi/2} \chi'\psi' d\theta \right) - \epsilon\sigma (T_c^4 - T_t^4) + Q = 0 \tag{B2}$$

The integrals to be evaluated are

$$\int_0^{\pi/2} \chi d\theta \tag{B3}$$

$$\int_0^{\pi/2} \chi' d\theta \tag{B4}$$

$$\int_0^{\pi/2} \chi\psi d\theta \tag{B5}$$

$$\int_0^{\pi/2} \chi' \psi' d\theta \tag{B6}$$

If the value of X in equation (B3) is replaced by its definition (from list of symbols), equation (B3) becomes

$$\int_0^{\pi/2} \left[e^{-s^2 \sin^2 \theta} + \sqrt{\pi}\, s \sin \theta + \sqrt{\pi}\, s \sin \theta \, \text{erf}(s \sin \theta) \right] d\theta \quad \text{(B7)}$$

The first term of this integral can be evaluated by setting

$$s = 2x \text{ and } \cos 2\theta = z$$

Then, $d\theta = -\dfrac{dz}{2 \sin 2\theta}$ and the limits become

$$z = 1 \text{ when } \theta = 0$$

$$z = -1 \text{ when } \theta = \frac{\pi}{2}$$

Thus we can write

$$\int_0^{\pi/2} e^{-s^2 \sin^2 \theta}\, d\theta = \frac{e^{-x}}{2} \int_{-1}^1 \frac{e^{xz}}{\sqrt{1-z^2}}\, dz \quad \text{(B8)}$$

Now, by definition (cf., equation (11), p. 46, reference 18), the modified Bessel function of order n can be written as

$$I_n(x) = \frac{1}{\sqrt{\pi}\, \Gamma[n+(1/2)]} \left(\frac{x}{2} \right)^n \int_{-1}^1 e^{\pm xz} (1-z^2)^{n-(1/2)}\, dz \quad \text{(B9)}$$

Then

$$I_0(x) = \frac{1}{\sqrt{\pi}\, \Gamma(1/2)} \int_{-1}^1 \frac{e^{xz}}{\sqrt{1-z^2}}\, dz$$

and since

$$\Gamma \left(\frac{1}{2} \right) = \sqrt{\pi}$$

the first term of integral (B3) becomes

$$\frac{\pi}{2} e^{-s^2/2} I_0 \left(\frac{s^2}{2}\right) \tag{B10}$$

The second term (cf., equation (B7)) is

$$\sqrt{\pi} s \int_0^{\pi/2} \sin \theta \, d\theta = \sqrt{\pi} s \tag{B11}$$

The third term of equation (B7) is

$$\sqrt{\pi} s \int_0^{\pi/2} \sin \theta \, \text{erf} (s \sin \theta) \, d\theta$$

which can be integrated by parts. Let

$$\text{erf} (s \sin \theta) = u$$

and

$$\sin \theta \, d\theta = dv$$

Then

$$du = \frac{2s}{\sqrt{\pi}} e^{-s^2 \sin^2 \theta} \cos \theta \, d\theta$$

and

$$v = -\cos \theta$$

Then, the integral becomes

$$\sqrt{\pi} s \left[-\cos \theta \, \text{erf} (s \sin \theta) \right]_0^{\pi/2} + 2s^2 \int_0^{\pi/2} \cos^2 \theta \, e^{-s^2 \sin^2 \theta} \, d\theta \tag{B12}$$

The bracketed term of equation (B12) is zero, leaving the second term yet to be evaluated. Make the substitutions

$$\cos^2 \theta = \frac{1 + \cos u}{2}$$

$$\sin^2 \theta = \frac{1 - \cos u}{2}$$

$$s^2 = 2x$$

Then

$$d\theta = \frac{du}{2}$$

and, replacing limits

$$\theta = 0 \qquad\qquad u = 0$$

$$\theta = \frac{\pi}{2} \qquad\qquad u = \pi$$

there results

$$2s^2 \int_0^{\pi/2} \cos^2 \theta \; e^{-s^2 \sin^2 \theta} \; d\theta = \frac{s^2}{2} \int_0^{\pi} (1 + \cos u) \; e^{-x(1 - \cos u)} \; du$$

$$= \frac{s^2 e^{-x}}{2} \int_0^{\pi} e^{-x \cos u} \; du + \frac{s^2 e^{-x}}{2} \int_0^{\pi} \cos u \; e^{x \cos u} \; du \qquad (B13)$$

Integral (B13) becomes, when substituting $z = \cos u$ and changing limits,

$$\frac{s^2 e^{-x}}{2} \int_{-1}^{1} \frac{e^{xz}}{\sqrt{1 - z^2}} \; dz + \frac{s^2 e^{-x}}{2} \int_{-1}^{1} \frac{z e^{xz}}{\sqrt{1 - z^2}} \; dz$$

$$= \frac{\pi s^2}{2} e^{-s^2/2} \left[I_0 \left(\frac{s^2}{2} \right) + I_1 \left(\frac{s^2}{2} \right) \right] \qquad (B14)$$

which is obtained by integrating the second term of (B14) by parts and substituting equation (B9). Then, the final value for integral (B3) is

$$\int_0^{\pi/2} X d\theta = \frac{\pi}{2} e^{-s^2/2} I_0 \left(\frac{s^2}{2} \right) + \sqrt{\pi} \; s + \frac{\pi s^2}{2} e^{-s^2/2} \left[I_0 \left(\frac{s^2}{2} \right) + I_1 \left(\frac{s^2}{2} \right) \right]$$

$$(B15)$$

Now, integrals (B4), (B5), and (B6) contain only terms which can be evaluated by the methods shown above by which integral (B3) was evaluated. The results are

$$\int_0^{\pi/2} \chi' d\theta = \frac{\pi}{2} e^{-s^2/2} I_0\left(\frac{s^2}{2}\right) - \sqrt{\pi}\, s + \frac{\pi s^2}{2} e^{-s^2/2}\left[I_0\left(\frac{s^2}{2}\right) + I_1\left(\frac{s^2}{2}\right)\right]$$

(B16)

$$\int_0^{\pi/2} \chi\psi\, d\theta = \pi\, e^{-s^2/2} I_0\left(\frac{s^2}{2}\right) + \frac{5}{2}\sqrt{\pi}\, s + \frac{5}{4}\pi\, s^2 e^{-s^2/2}\left[I_0\left(\frac{s^2}{2}\right) + I_1\left(\frac{s^2}{2}\right)\right]$$

(B17)

$$\int_0^{\pi/2} \chi'\psi'\, d\theta = \pi e^{-s^2/2} I_0\left(\frac{s^2}{2}\right) - \frac{5}{2}\sqrt{\pi}\, s + \frac{5}{4}\pi s^2 e^{-s^2/2}\left[I_0\left(\frac{s^2}{2}\right) + I_1\left(\frac{s^2}{2}\right)\right]$$

(B18)

In order to eliminate an excessive amount of writing, new variables are defined as follows:

$$Z_1 = \pi\, e^{-s^2/2} I_0\left(\frac{s^2}{2}\right)$$

(B19)

$$Z_2 = \pi\, s^2 e^{-s^2/2}\left[I_0\left(\frac{s^2}{2}\right) + I_1\left(\frac{s^2}{2}\right)\right]$$

(B20)

Values of the dimensionless variables Z_1 and Z_2 were computed from the tables of Bessel functions in reference 19. Then, equation (B21) is obtained by substitution of equations (B15) to (B20) into equation (B2).

$$\frac{Nv_m\alpha}{4\pi^{3/2}}(mU^2 - 4kT_c)(Z_1 + Z_2) + \frac{\alpha kTNv_m}{2\pi^{3/2}}\left(2Z_1 + \frac{5}{2}Z_2\right) - \epsilon\sigma(T_c^4 - T_t^4) + Q = 0 \quad (B21)$$

If $mv_m^2/2 = kT$, $kTN = p$, and $s = U/v_m$ are substituted into equation (B21), the following equation results:

$$2 \frac{T_c}{T} (Z_1 + Z_2) - \left[Z_1(s^2+2) + Z_2 \left(s^2 + \frac{5}{2} \right) \right] + \frac{2\pi^{3/2}}{p v_m \alpha} [\epsilon \sigma (T_c{}^4 - T_t{}^4) - Q] = 0 \qquad (B22)$$

which is the final energy exchange equation for a monatomic gas. An identical treatment of equation (13) for a diatomic gas gives

$$3 \frac{T_c}{T} (Z_1 + Z_2) - \left[Z_1(s^2+3) + Z_2 \left(s^2 + \frac{7}{2} \right) \right] + \frac{2\pi^{3/2}}{p v_m \alpha} [\epsilon \sigma (T_c{}^4 - T_t{}^4) - Q] = 0$$
$$(B23)$$

The groups $f(s) = Z_1(s^2+3) + Z_2 \left(s^2 + \frac{7}{2} \right)$, $g(s) = 3(Z_1 + Z_2)$, $f^0(s) = Z_1(s^2+2) + Z_2 \left(s^2 + \frac{5}{2} \right)$, and $g^0(s) = 2(Z_1 + Z_2)$ are tabulated in the following table:

s	f(s)	g(s)	f^0(s)	g^0(s)
0.2	9.80271	9.61234	6.59860	6.40823
.4	10.94784	10.16410	7.55981	6.77607
.6	12.89399	11.04924	9.21092	7.36616
.8	15.69746	12.22282	11.62319	8.14855
1.0	19.43609	13.63288	14.89180	9.08859
1.2	24.20781	15.22758	19.13179	10.15172
1.4	30.12863	16.96068	24.47507	11.30712
1.6	37.32923	18.79408	31.06454	12.52939
1.8	45.95230	20.69872	39.05273	13.79915
2.0	56.14932	22.65358	48.59807	15.10239
2.2	68.07771	24.64392	59.86307	16.42928
2.4	81.89947	26.65990	73.01284	17.77327
2.6	97.77902	28.69470	88.21412	19.12980
2.8	115.88287	30.74382	105.63493	20.49588
3.0	136.37821	32.80398	125.44355	21.86932
3.2	159.43361	34.87300	147.80928	23.24867
3.4	185.21769	36.94914	172.90131	24.63276
3.6	213.89927	39.03112	200.88890	26.02075
3.8	245.64801	41.11800	231.94201	27.41200
4.0	280.63340	43.20904	266.23039	28.80603
4.2	319.02474	45.30354	303.92365	30.20236
4.4	360.99204	47.40108	345.19168	31.60072
4.6	406.70528	49.50126	390.20486	33.00084
4.8	456.33364	51.60366	439.13242	34.40244
5.0	510.04756	53.70808	492.14487	35.80539
5.2	568.01730	55.81428	549.41254	37.20952
5.4	630.41182	57.92200	611.10449	38.61467
5.6	697.40229	60.03114	677.39191	40.02076

APPENDIX C

THE DRAG DUE TO IMPINGING MOMENTUM ON A TRANSVERSE CYLINDER IN FREE-MOLECULE FLOW

The differential momentum imparted, by the impact of impinging molecules, to the front and rear sides of a body located in a free-molecule flow field is (cf., references 1, 2, and 3)

$$dG_1 = \frac{\beta^3 mN}{\pi^{3/2}} \left\{ \int_{-\infty}^{\infty}\int_{-\infty}^{\infty}\int_{0}^{\infty} (l_x c_x + l_y c_y + l_z c_z)\, c_x\, e^{-\beta^2[(c_x-U_x)^2+(c_y-U_y)^2+(c_z-U_z)^2]}\, dc_x dc_y dc_z \right.$$
$$\left. - \int_{-\infty}^{\infty}\int_{-\infty}^{\infty}\int_{-\infty}^{0} (l_x c_x + l_y c_y + l_z c_z)\, c_x\, e^{-\beta^2[(c_x-U_x)^2+(c_y-U_y)^2+(c_z-U_z)^2]}\, dc_x dc_y dc_z \right\} dA \tag{C1}$$

In equation (C1), l_x, l_y, l_z are the cosines of the angle between the coordinate axes and the direction of the momentum force. Now let θ be the angle of attack of the element, that is, the angle between the mass velocity U and the plane of the plate. Then the drag force is in the direction of U and the following relations can be derived:

$$\left. \begin{aligned} l_x &= \sin\theta & U_x &= U\sin\theta \\ l_y &= -\cos\theta & U_y &= -U\cos\theta \\ l_z &= 0 & U_z &= 0 \end{aligned} \right\} \tag{C2}$$

Then, integration of equation (C1) and substitution of the relations of equation (C2) yield

$$dG_i = \frac{\rho U^2}{2} \left[\frac{2}{\pi^{1/2}} \frac{e^{-s^2 \sin^2 \theta}}{s} + 2 \sin \theta \, \text{erf} \, (s \sin \theta)\left(1 + \frac{1}{2s^2}\right)\right] dA \quad (C3)$$

It is remarkable that a purely analytic solution for this type flow leads to a simple equation of the type of (C3) in which the bracketed term is a dimensionless function of molecular speed ratio and which may be interpreted as an ordinary drag coeffient.

In order to obtain the drag force on a transverse cylinder due to impinging momentum, equation (C3), which was derived for an elemental plane area, must be integrated over the surface of the cylinder. To this end, dA is written as

$$dA = rLd\theta \quad (C4)$$

Then, for the cylinder, the impinging drag force is

$$G_i = 2rL \left(\frac{\rho U^2}{2}\right) \int_0^{\pi/2} \left[\frac{2e^{-s^2 \sin^2 \theta}}{\pi^{1/2}s} + 2 \sin \theta \, \text{erf}(s \sin \theta) \left(1 + \frac{1}{2s^2}\right) \right] d\theta \quad (C5)$$

This integral can be evaluated by the methods shown in appendix B. The final value for the drag force due to impinging molecules is

$$G_i = 2rL \left(\frac{\rho U^2}{2}\right)\frac{\pi^{1/2}e^{-s^2/2}}{s}\left\{I_0\left(\frac{s^2}{2}\right) + \left(\frac{1+2s^2}{2}\right)\left[I_0\left(\frac{s^2}{2}\right) + I_1\left(\frac{s^2}{2}\right)\right]\right\} \quad (C6)$$

Thus, there results from equation (C6) an impinging drag coefficient based on the projected area of the cylinder, which has the value

$$C_{D_i} = \frac{\pi^{1/2}e^{-s^2/2}}{s}\left\{I_0\left(\frac{s^2}{2}\right) + \left(\frac{1+2s^2}{2}\right)\left[I_0\left(\frac{s^2}{2}\right) + I_1\left(\frac{s^2}{2}\right)\right]\right\} \quad (C7)$$

REFERENCES

1. Ashley, Holt: Application of the Theory of Free Molecule Flow to Aeronautics. Inst. Aero. Sci., Preprint 164, 1949.

2. Tsien, Hsue-Shen: Superaerodynamics, Mechanics of Rarefied Gases. Jour. Aero. Sci., vol. 13, no. 12, Dec. 1946, pp. 653-664.

3. Heineman, M.: Theory of Drag in Highly Rarefied Gases, Communications on Pure and Applied Mathematics. Vol. 1, no. 3, Sept. 1948, pp. 259-273.

4. Stalder, Jackson R., and Jukoff, David: Heat Transfer to Bodies Traveling at High Speed in the Upper Atmosphere. NACA TN 1682, 1948.

5. Whipple, Fred L.: Meteors and the Earth's Upper Atmosphere. Review of Modern Physics, vol. 15-16, Oct. 1943, pp. 246-264.

6. Epstein, Paul S.: On the Resistance Experienced by Spheres in Their Motion Through Gases. Physical Review, vol. 23, no. 6, June 1924, pp. 710-733.

7. Loeb, Leonard B.: Kinetic Theory of Gases. McGraw Hill Book Co., Inc., N.Y., 2d ed., 1934.

8. Kennard, Earle H.: Kinetic Theory of Gases, With an Introduction to Statistical Mechanics. McGraw Hill Book Co., Inc., N.Y., 1st ed., 1938.

9. Cronvich, Lester L.: A Numerical-Graphical Method of Characteristics for Axially Symmetric Isentropic Flow. Jour. Aero. Sci., vol. 15, no. 3, Mar. 1948, pp. 155-162.

10. Dushman, Saul: Scientific Foundations of Vacuum Technique. John Wiley and Sons, N.Y., 1949.

11. Mann, W. R., and Schaaf, S. A.: Vacuum Gage Time Lags Due to Outgassing. University of California, Dept. of Engineering, Rep. No. HE-150-26, Sept. 1947.

12. Schaaf, S. A., and Cyr, R. R.: Time Constants for Vacuum Gage Systems. University of California, Dept. of Engineering, No. HE-150-42, Mar. 1948.

13. Jones, Robert T., and Margolis, Kenneth: Flow Over a Slender Body of Revolution at Supersonic Velocities. NACA TN 1081, 1946.

14. Chambré, P. L.: The Theory of the Impact Tube in a Viscous Compressible Gas. University of California, Dept. of Engineering, Rep. No. HE-150-50, Nov. 1948.

15. Williams, Thomas W., and Benson, James M.: Preliminary Investigation of the Use of Afterglow for Visualizing Low-Density Compressible Flows. NACA TN 1900, 1949.

16. Schamberg, Richard: The Fundamental Differential Equations and the Boundary Conditions for High-Speed Slip-Flow and Their Application to Several Specific Problems. Thesis, GALCIT, 1947. (Thesis submitted in partial fulfillment of the requirements for the degree of Doctor of Philosophy.)

17. Lamb, Horace: Hydrodynamics. Dover Publications, N.Y., 6th ed., 1945.

18. Gray, Andrew, and Mathews, G. B.: A Treatise on Bessel Functions and Their Applications to Physics. MacMillan and Co., Ltd., London, Eng., 1931.

19. Watson, G. N.: A Treatise on the Theory of Bessel Functions. The University Press, Cambridge, Eng., 1944.

TABLE I.— WIND—TUNNEL—CALIBRATION DATA

Nozzle number	Design Mach number	Test gas	Test chamber static pressure (microns Hg)	Stagnation pressure (mm Hg)	Test[1] Mach number
1	4.5	N_2	71.0	2.7	2.49
		N_2	121.0	5.0	2.78
		He	18.7	.70	.55
		He	51.5	2.2	2.08
		He	90.0	3.8	2.37
2	3.6	N_2	70.0	1.2	2.07
		N_2	117.0	2.2	2.25
		He	51.7	.95	1.57
		He	89.2	1.7	1.75
3	3.0	N_2	71.0	.90	1.85
		He	31.0	.35	.73
		He	45.0	.55	1.00
4	3.11	He	20.0	.19	.89
		He	54.7	.55	1.67
		He	79.5	.70	1.68
		He	103.0	.90	1.73
		He	119.0	1.05	1.79
		He	137.0	1.20	1.83
5	2.64	He	20.0	.17	.78
		He	41.6	.30	1.23
		He	61.6	.40	1.36
		He	77.8	.45	1.44

[1]Average Mach number over center half inch of stream.

TABLE II.— TEST DATA

Nozzle number	Test gas	Mach number[1]	Test–chamber static pressure (microns Hg)	Stream static pressure (microns Hg)	Stagnation pressure (mm of Hg)	Stagnation temperature (°F)	Test–chamber surface temperature (°F)	Model temperatures			Model drag (milligrams)
								Iron end (°F)	Center point (°F)	Constantan end (°F)	
1	N₂	2.49	71.0	72.8	2.70	73.0	72.6	101.3	127.7	95.0	12.2–12.1
	N₂	2.78	120.0	120.2	5.00	73.0	72.2	94.0	119.0	87.2	21.7
	He	.55	18.0	19.5	.70	70.2	70.0	80.0	87.0	78.5	1.0–0.8
	He	2.08	51.0	49.4	2.15	72.2	70.2	123.7	189.0	117.0	4.8–4.5
	He	2.37	89.0	95.6	4.00	64.0	62.2	120.0	211.0	100.2	15.5–16.0
2	N₂	2.07	71.6	74.4	1.20	75.5	75.2	103.3	131.7	96.5	8.8
	N₂	2.25	119.0	132.7	2.20	74.7	75.2	95.7	122.7	90.2	18.5–17.5
	He	1.57	53.5	52.0	1.00	75.5	75.5	105.7	141.5	98.0	4.8–4.7
	He	1.75	91.0	91.0	1.70	65.0	67.5	114.4	183.3	100.6	8.7
3	N₂	1.85	68.7	68.7	.90	75.0	74.4	101.7	129.5	95.5	6.8–6.7
	He	.73	32.0	33.0	.35	76.2	74.0	82.5	93.7	78.5	1.7–1.5
	He	1.00	44.3	46.5	.60	67.4	68.7	87.6	110.5	81.4	2.7
4	He	.89	22.6	22.6	.19	68.5	74.7	80.7	87.5	78.2	1.1–1.2
	He	1.67	55.0	55.0	.50	74.0	74.4	101.0	132.0	93.7	3.5–3.6
	He	1.68	78.5	78.5	.70	68.2	69.4	107.0	162.5	95.5	7.0–6.7
	He	1.73	102.0	102.1	.90	70.7	70.8	110.7	174.5	97.5	10.4–10.0
	He	1.79	117.0	122.1	1.05	71.2	71.5	108.7	175.7	95.0	12.6–12.4
	He	1.83	130.0	135.0	1.15	70.8	71.2	106.3	173.5	92.4	14.7–14.5
5	He	.78	18.6	18.6	.15	73.7	74.3	76.6	80.5	74.8	0.75
	He	1.23	43.5	46.0	.30	76.3	74.3	94.2	117.7	88.2	2.85–2.7
	He	1.36	63.6	62.5	.40	74.2	74.3	102.7	140.3	94.5	4.4–4.2
	He	1.44	80.5	80.5	.47	73.3	74.8	105.0	147.8	97.0	6.0–5.8

[1]Average Mach number over center half inch of stream.

NACA

To atmosphere

Mechanical vacuum pump

Oil diffusion pumps

Settling chamber

Surge chamber

Test chamber

Nozzle

↑ Test gas

NACA
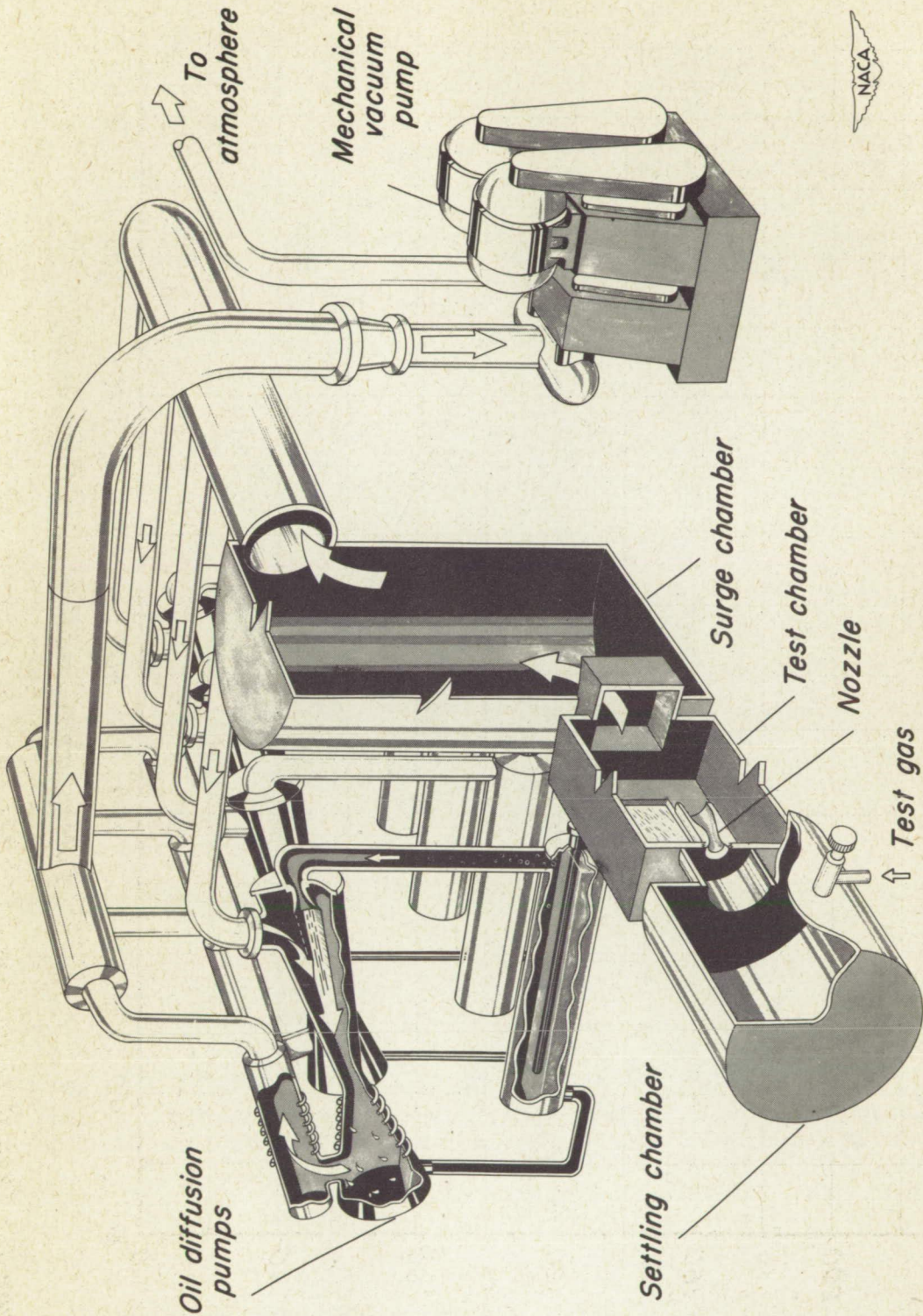
Figure 1.- Ames low-density wind tunnel.
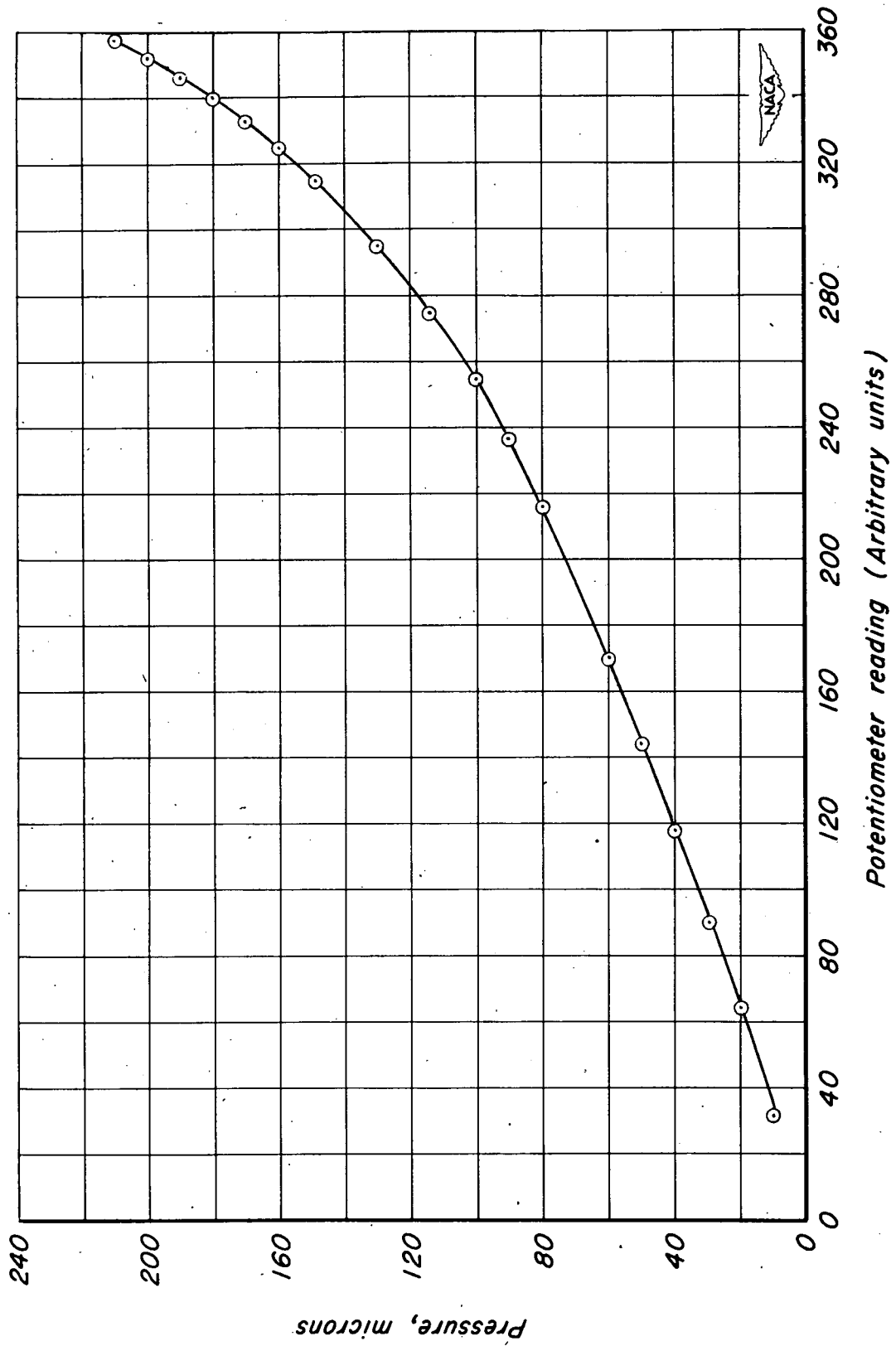
Figure 2.- Typical calibration of Pirani gage in nitrogen gas.

From traversing
mechanism

Spherical head impact-
pressure probe

Vacuum oil
manometer

0.013"d. $\frac{1}{8}$"d.

$\frac{1}{8}$"d. $\frac{1}{16}$"d.

Outgassing
heater

NACA
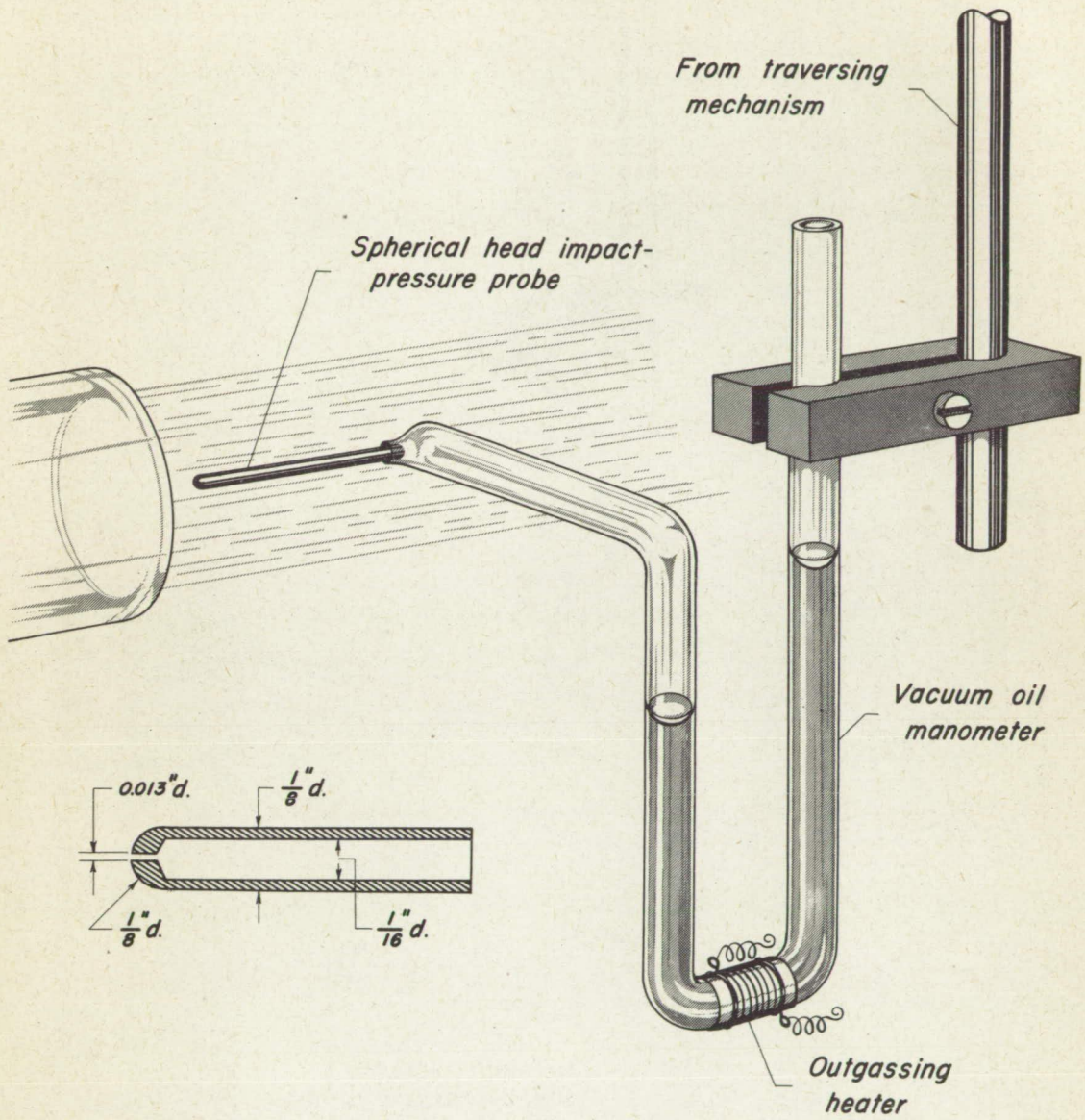
Figure 3. – Impact - pressure - measuring system.

From traversing mechanism

4 mm bore stopcock

Pirani tube

Nozzle

0.10-inch-diameter
static-pressure probe
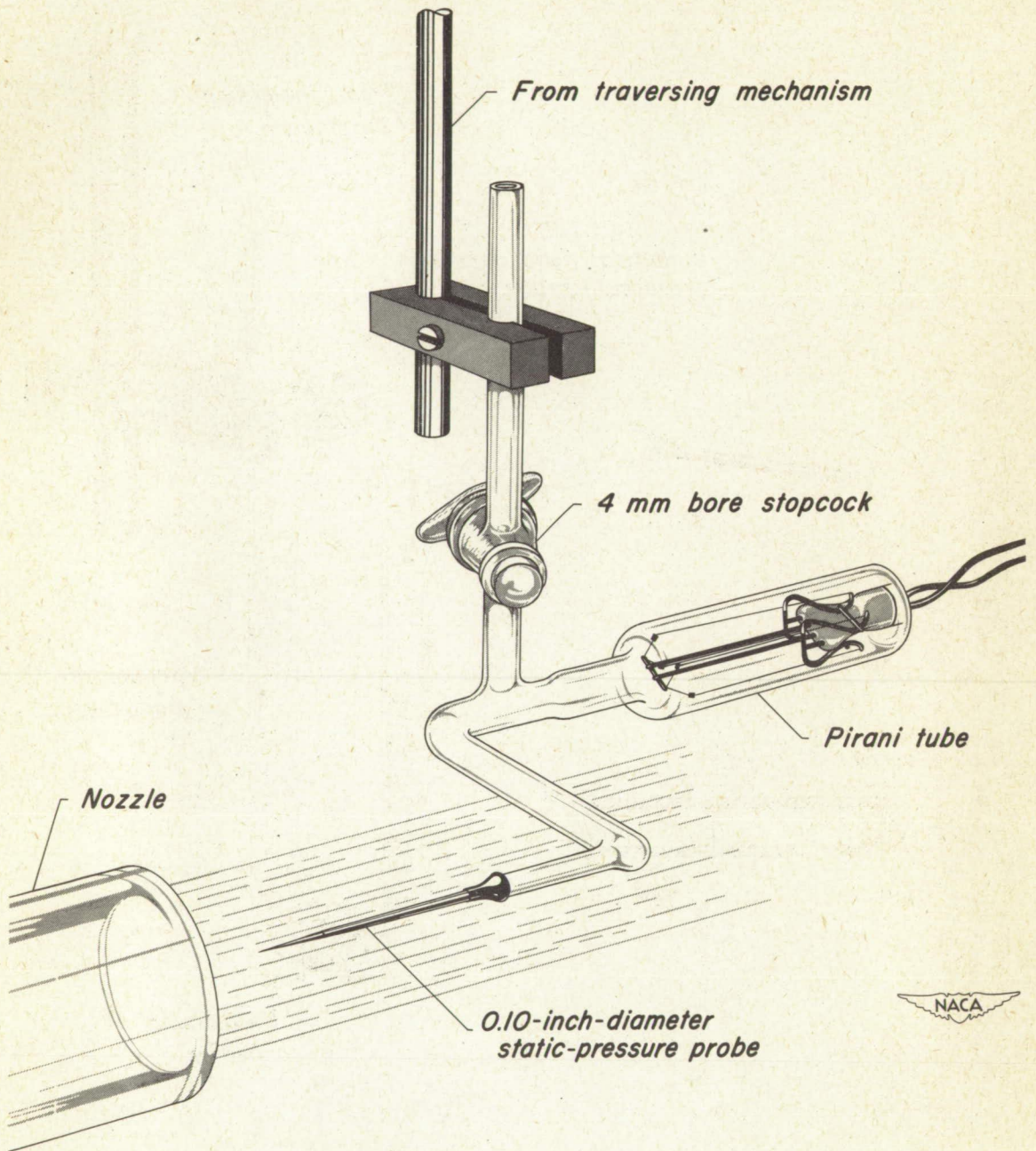
Figure 4.– Static-pressure-measuring system.

Note: All dimensions given in inches

x	d
0	0
0.05	0.019
.10	.036
.15	.051
.20	.064
.25	.075
.30	.084
.35	.091
.40	.096
.45	.099
.50	.100
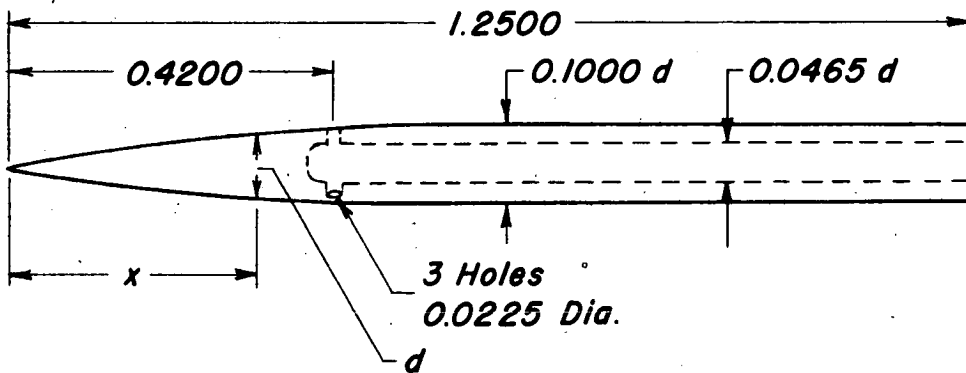
Figure 5.— Static-pressure probe used in the tests.
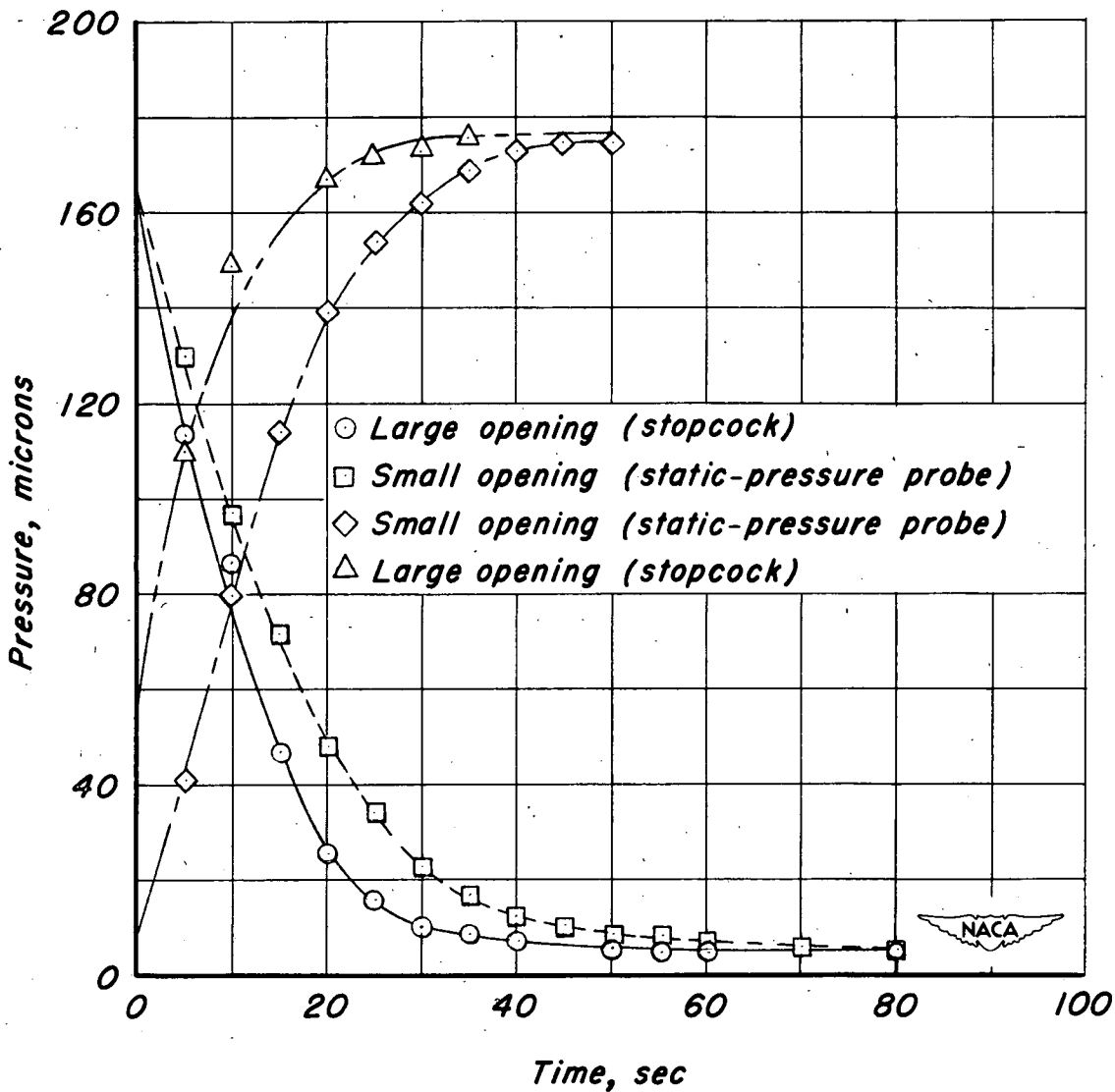
Figure 6.- Time response of the static-pressure-measuring system.
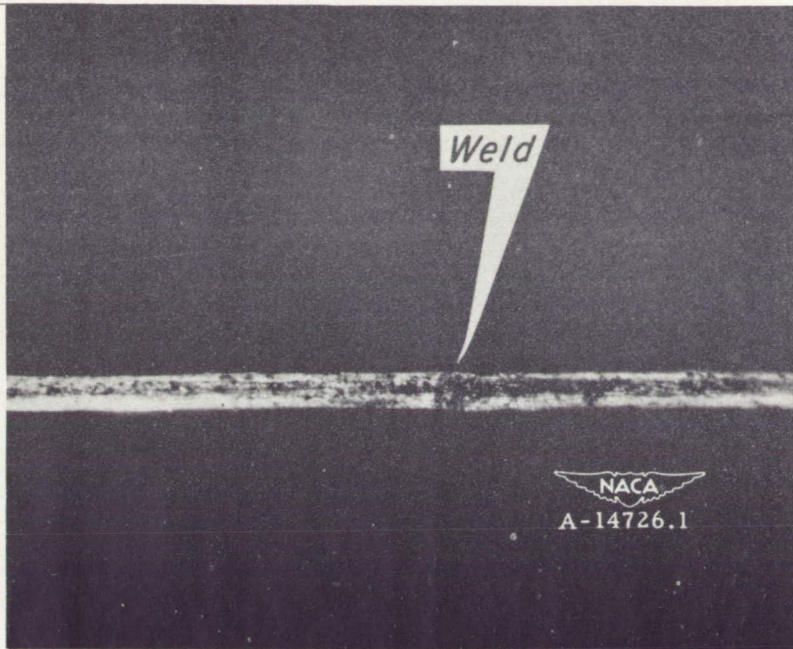
Figure 7.— Micro—photograph of model showing weld at junction of iron and constantan. Enlarged 60 times.
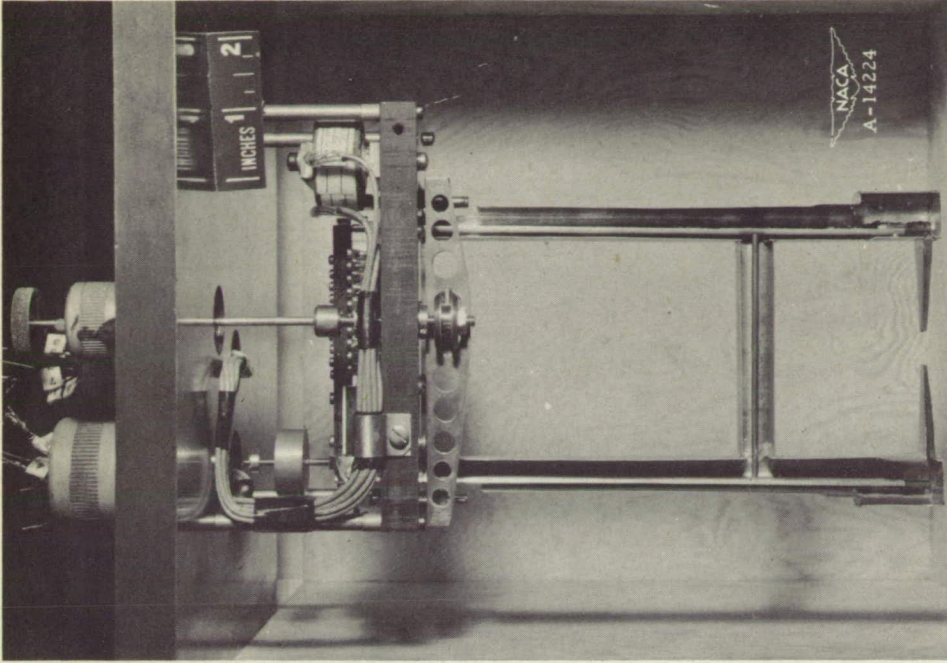
(b) Rear view.
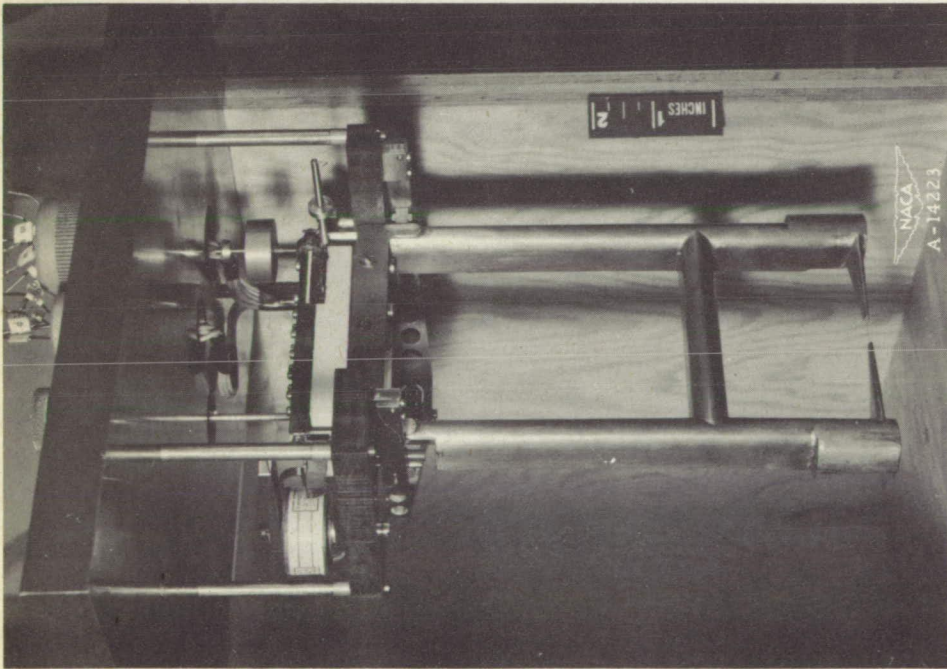
(a) Front view.

Figure 8.— Photograph of drag balance showing force shields.
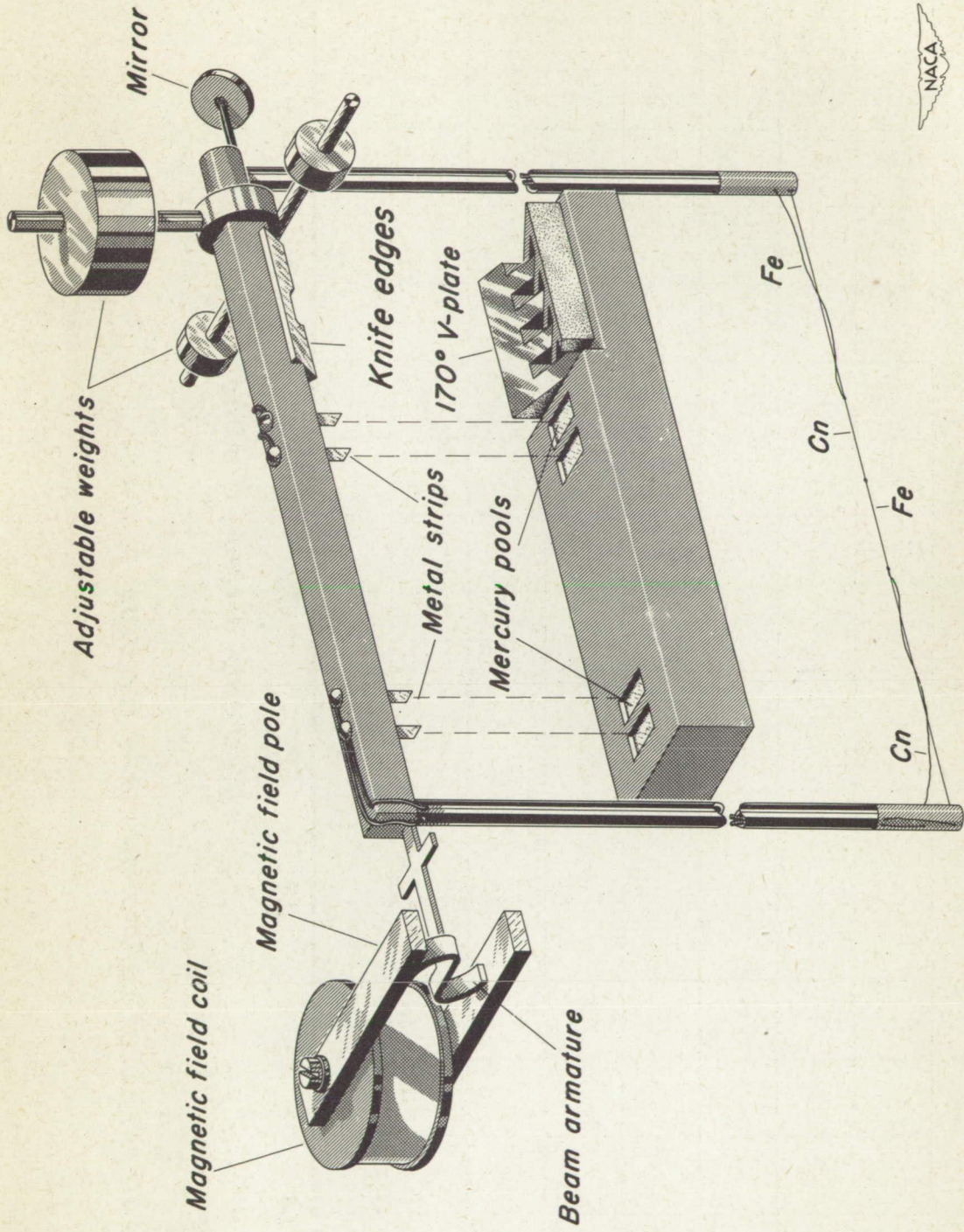
Figure 9.- Diagrammatic sketch of drag balance.
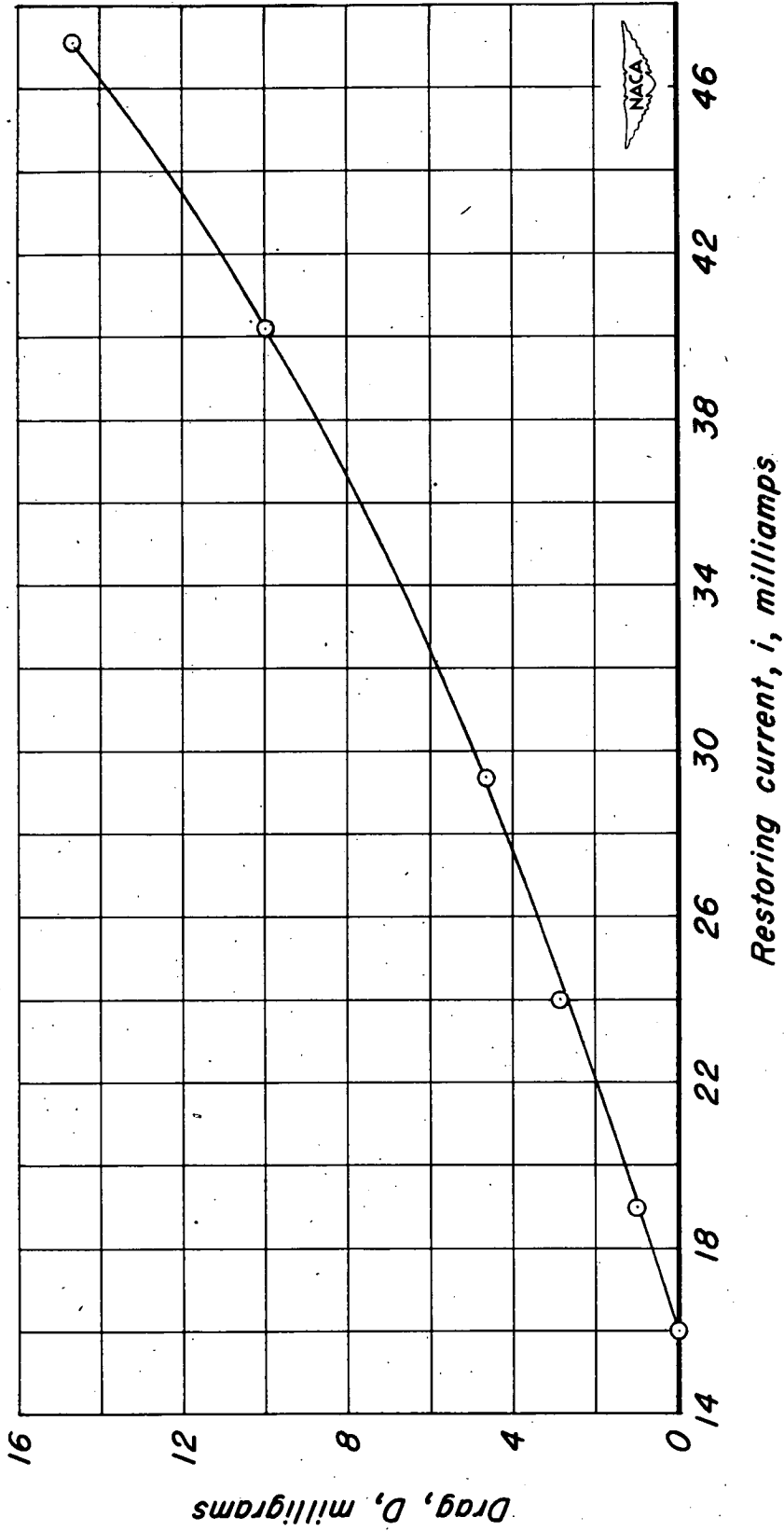
Figure 10.— Typical calibration curve for drag balance.
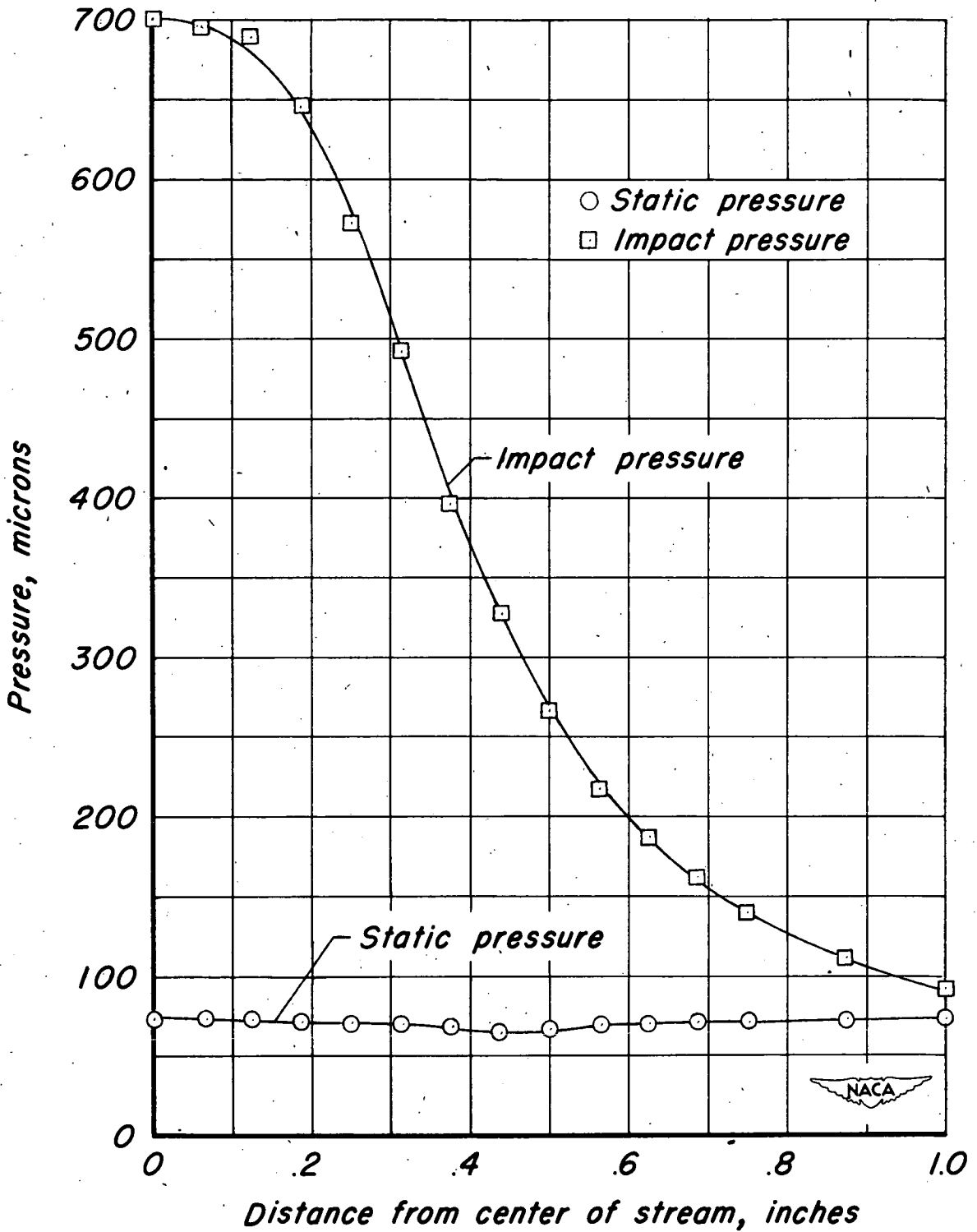
Figure 11.– Variation of impact and static pressure with
nozzle radius for nozzle number 1 using nitrogen gas.
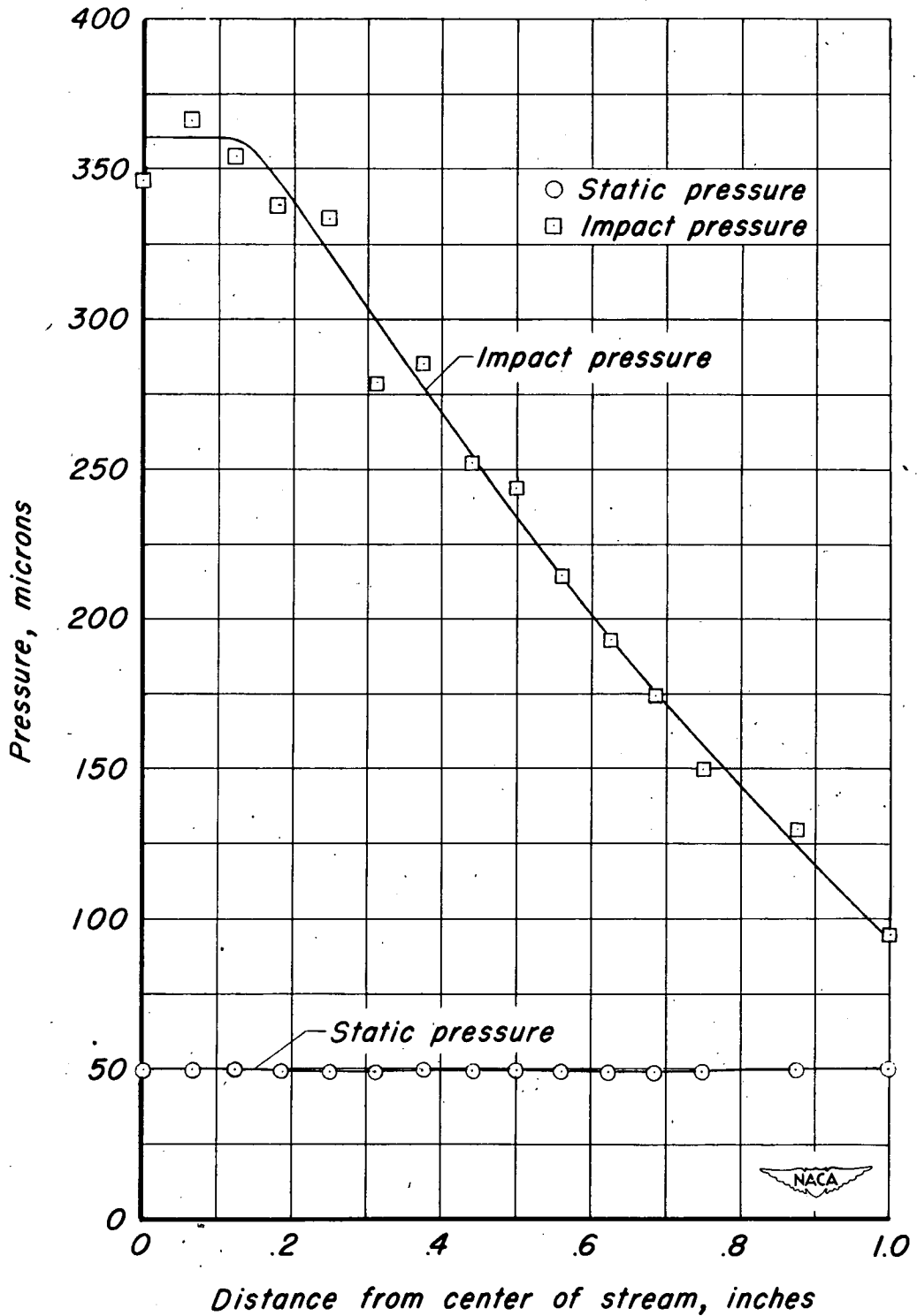
Figure 12.– Variation of impact and static pressure with
nozzle radius for nozzle number 1 using helium gas.
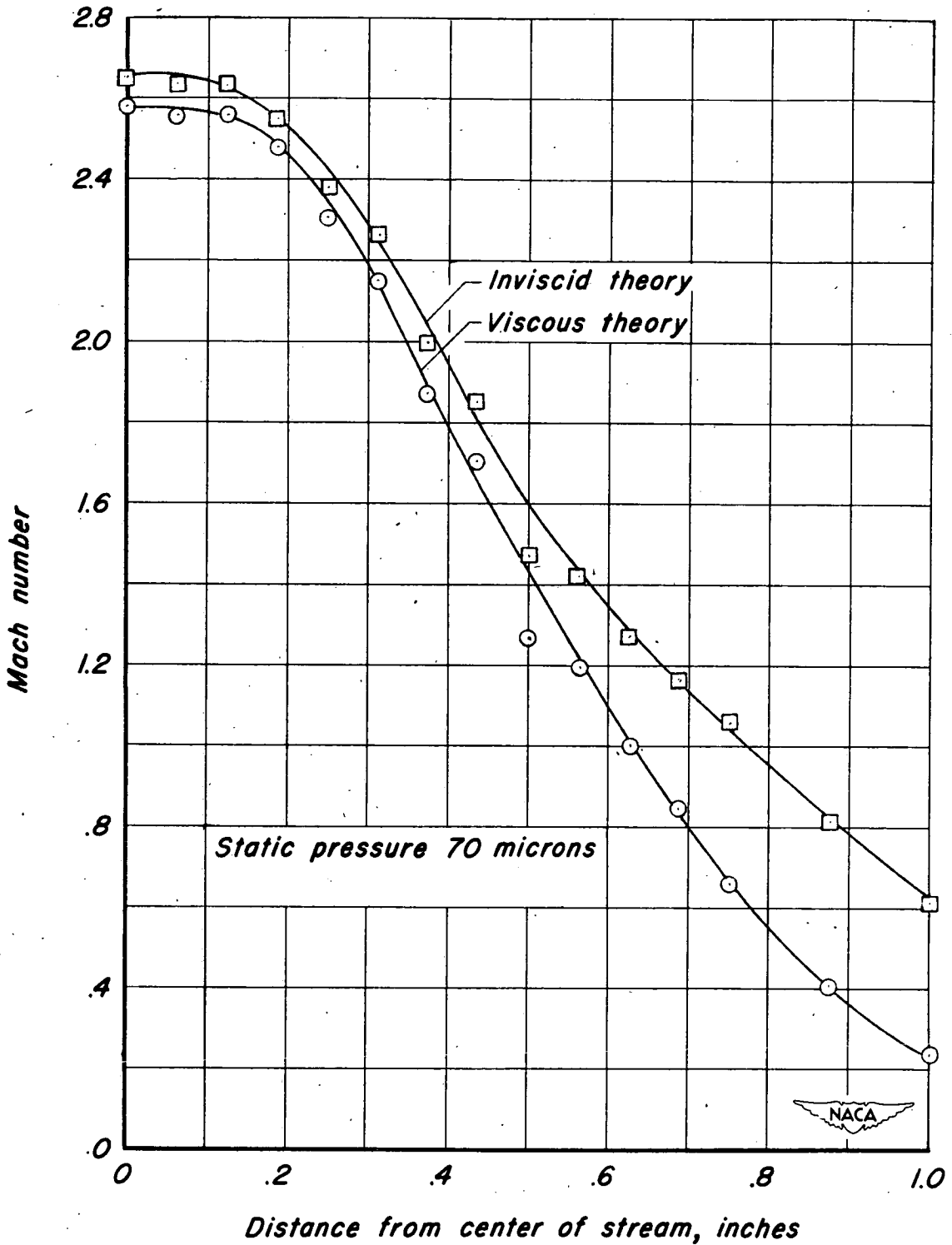
Figure 13.— Comparison of Mach number distribution in nozzle
number 1 as calculated with and without ·viscous correction,
test gas, nitrogen .
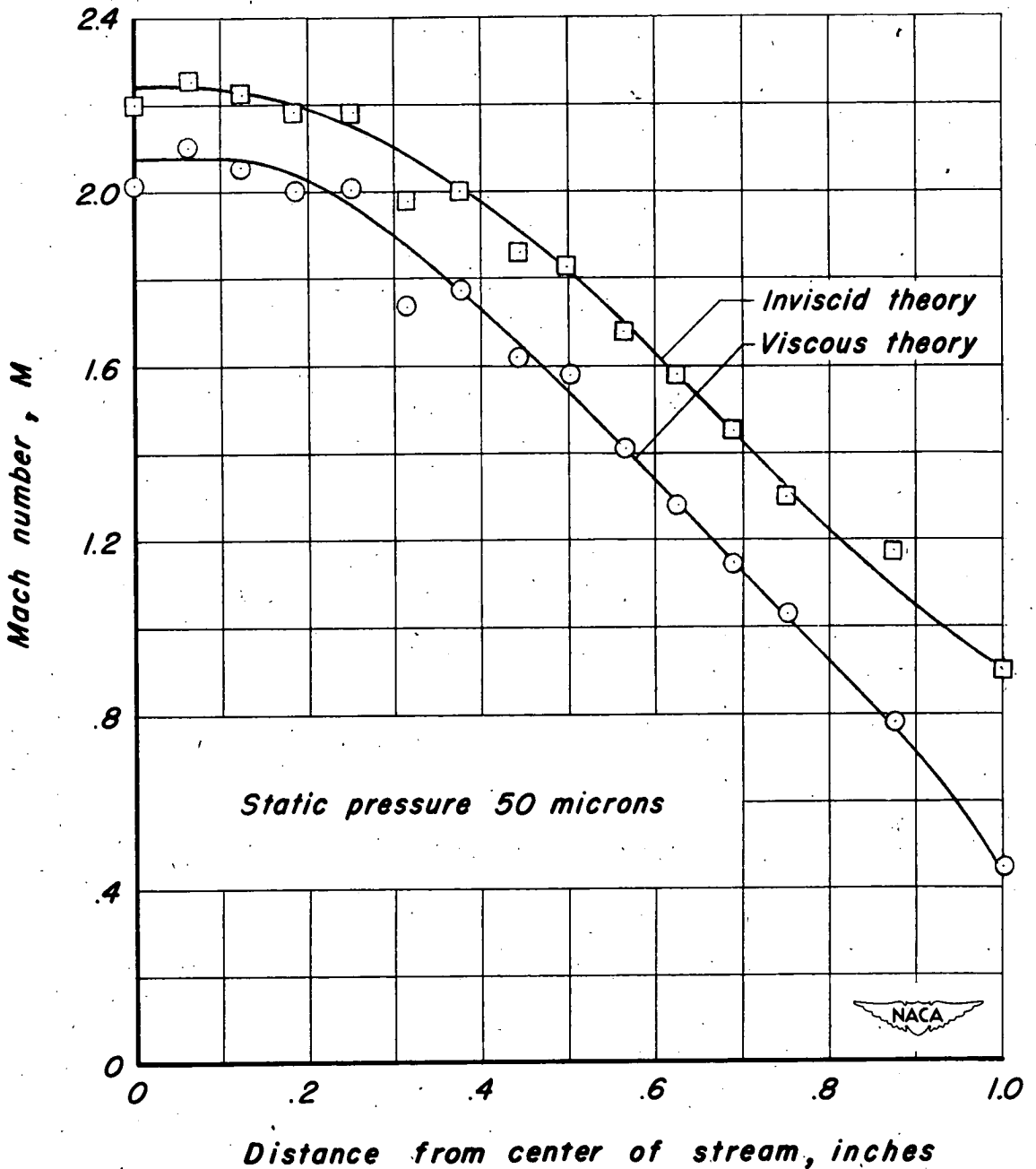
Figure 14.- Comparison of Mach number distribution in nozzle number 1 as calculated with and without viscous correction, test gas, helium.

Figure 15.— Shock wave from 5° half-angle wedge at pressure of 114 microns as seen with nitrogen glow discharge.

Page intentionally left blank
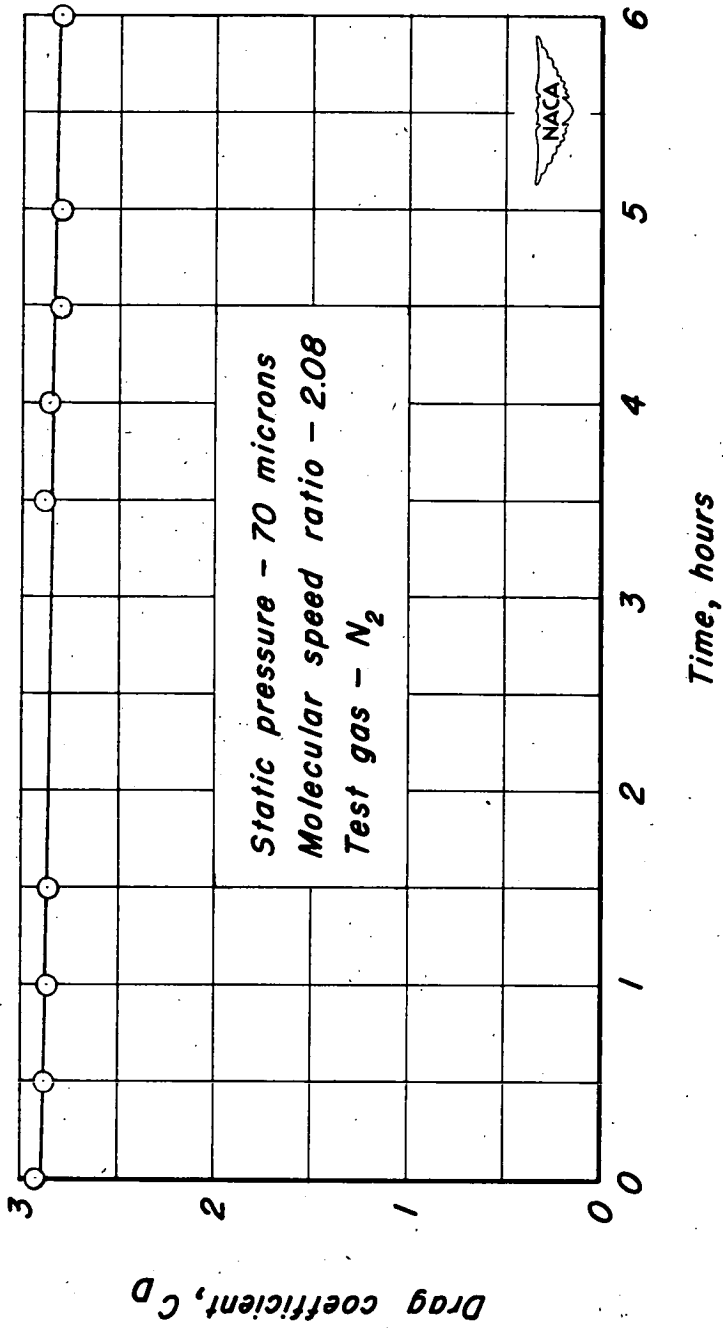
Figure 16.— Variation of measured drag coefficient with time.
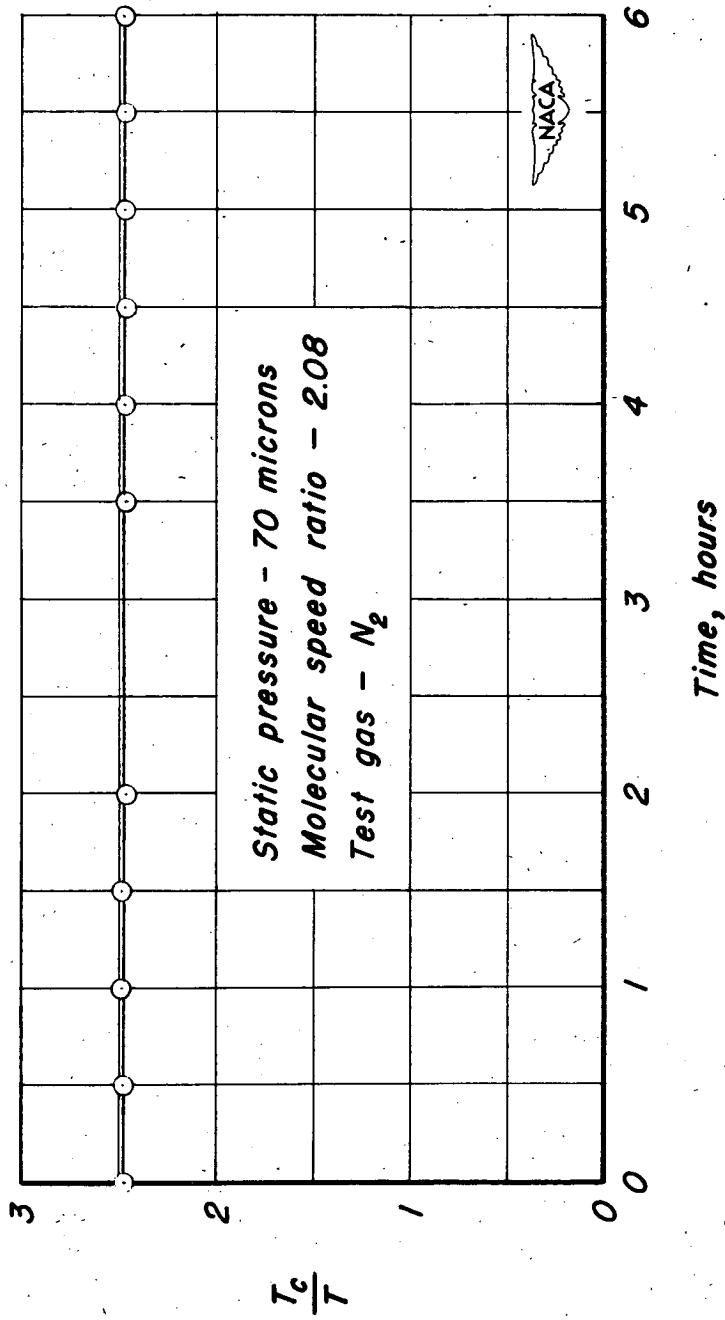
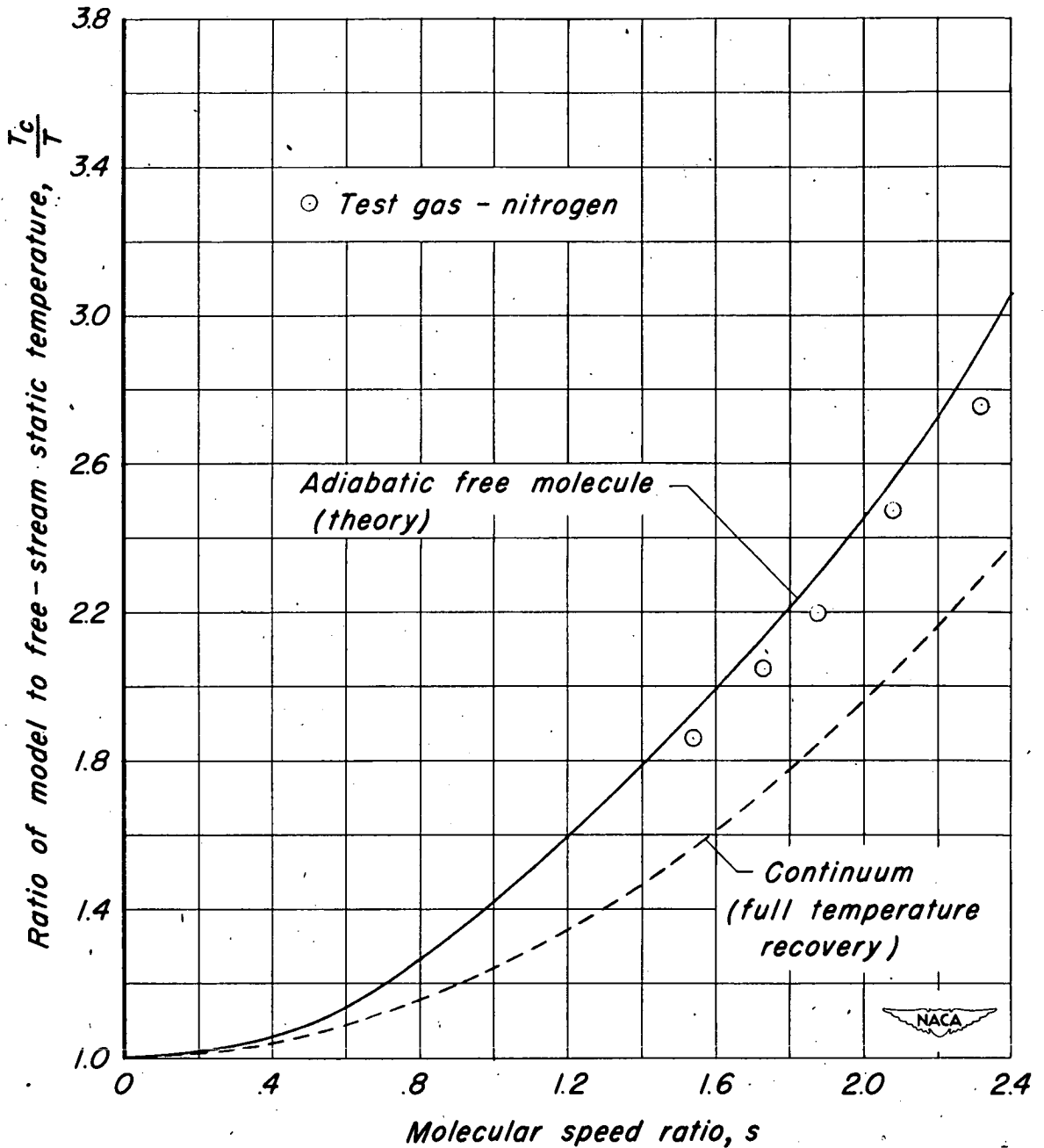Figure 17.- Variation of the ratio of model to free-stream temperature, T_c/T with time.
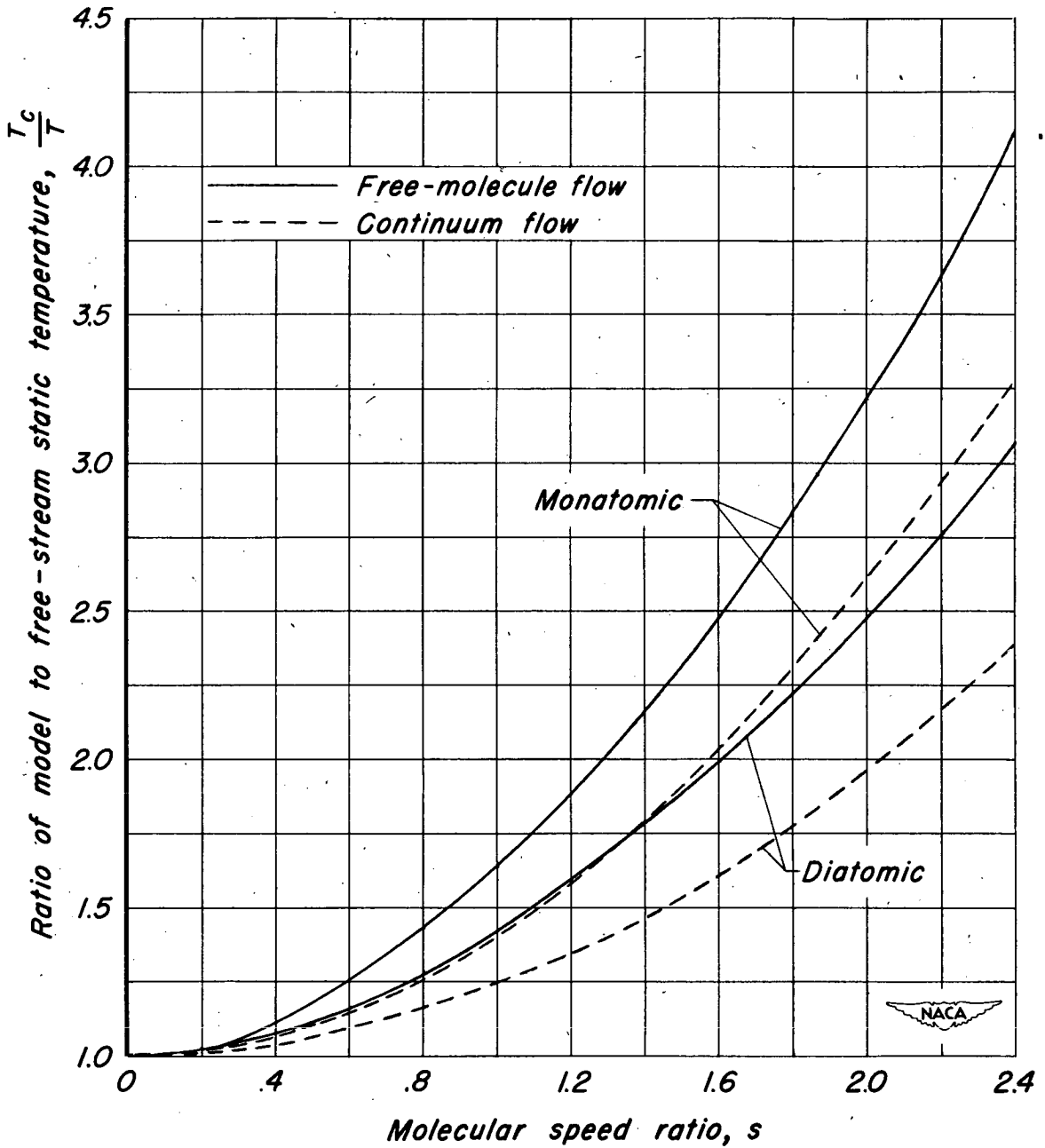
Figure 18.- Variation of the ratio of cylinder temperature to free-stream static temperature, with molecular speed ratio for an adiabatic cylinder in free-molecule flow.
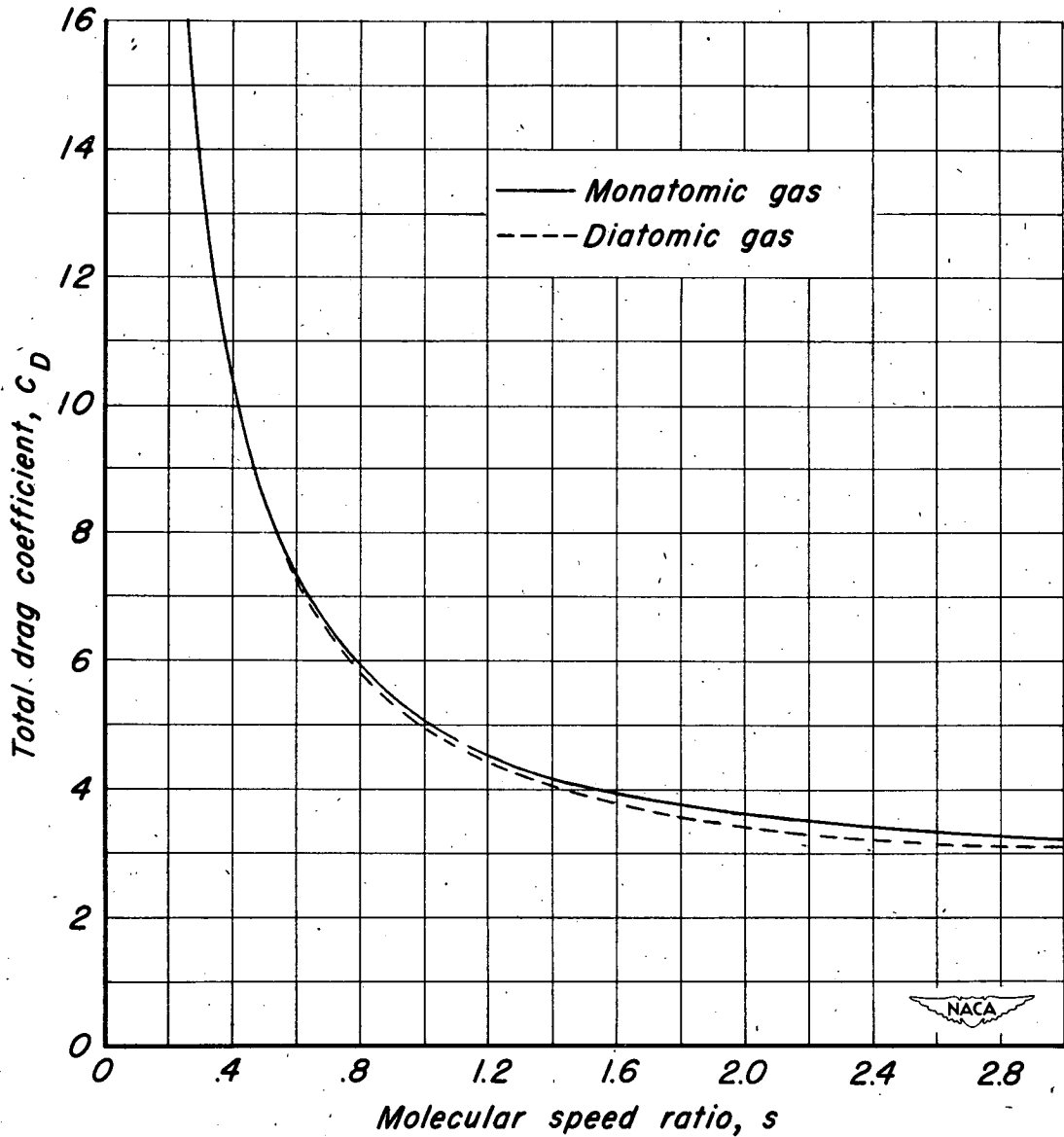
Figure 19.— The total drag coefficient for an insulated transverse cylinder in a free-molecule flow as a function of the molecular speed ratio, s.

Figure 20.- Variation of the ratio of model temperature to free-stream static temperature with molecular speed ratio for a diatomic gas.
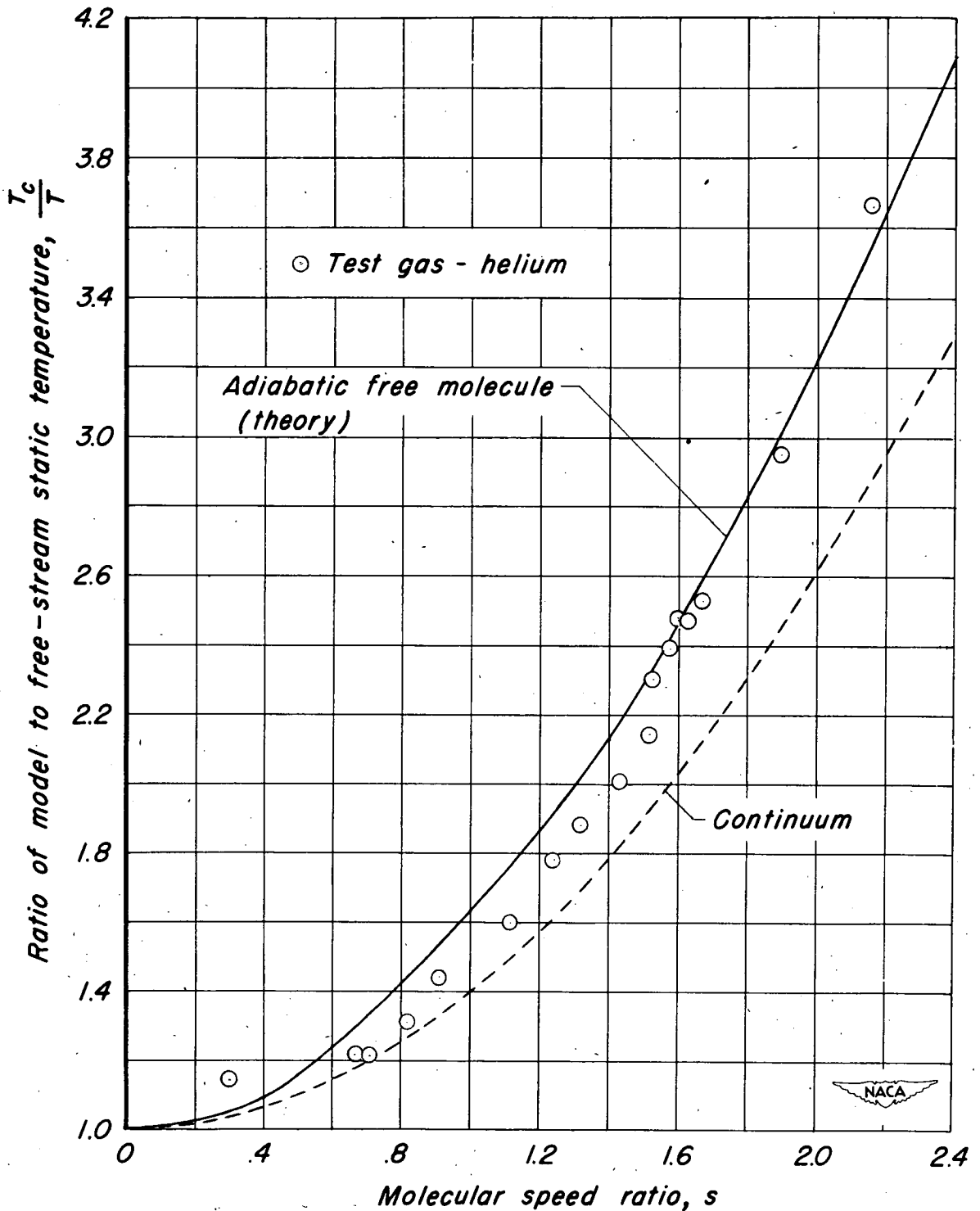
Figure 21.— Variation of the ratio of model temperature to free-
stream static temperature with molecular speed ratio for a
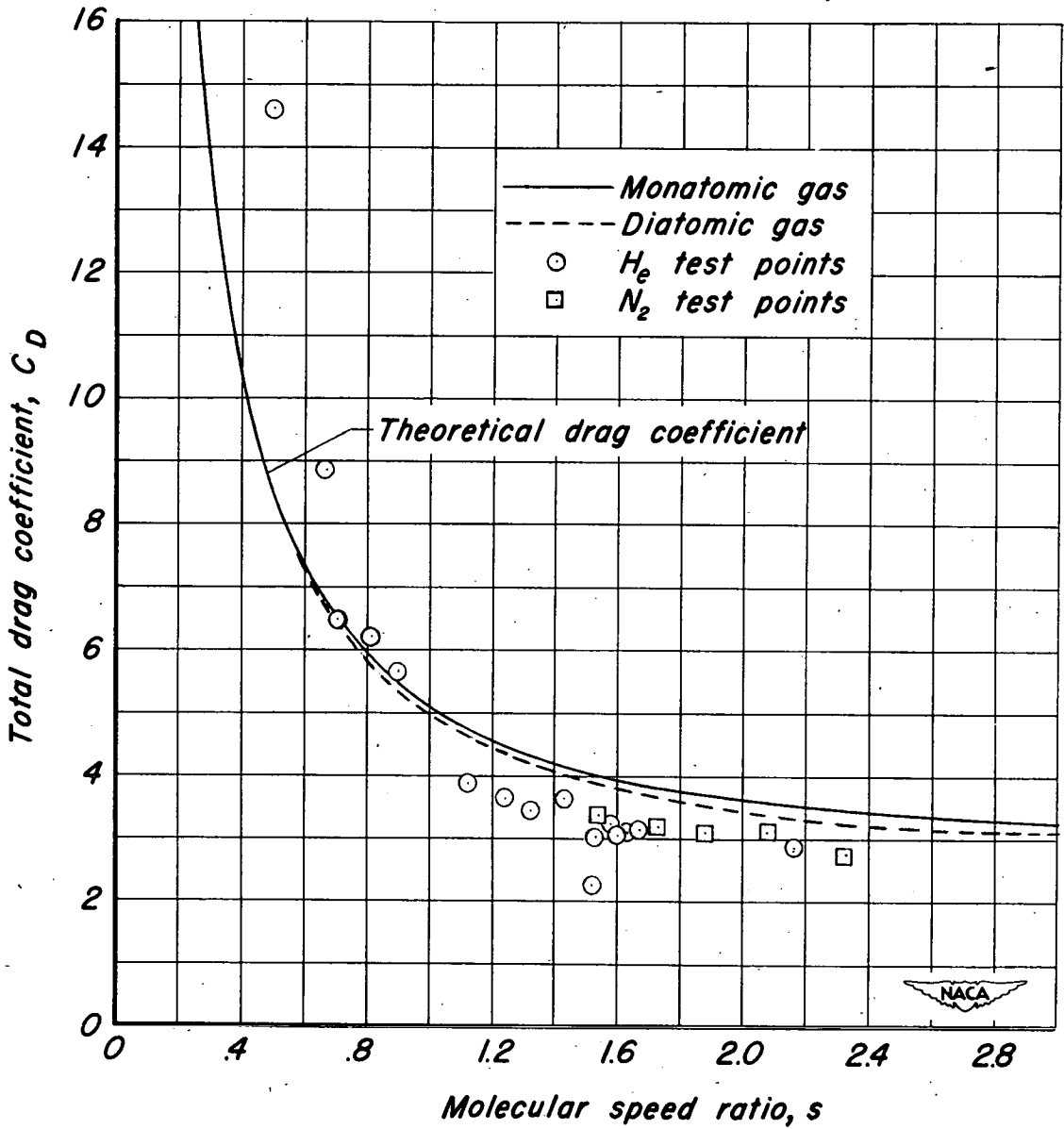monatomic gas.

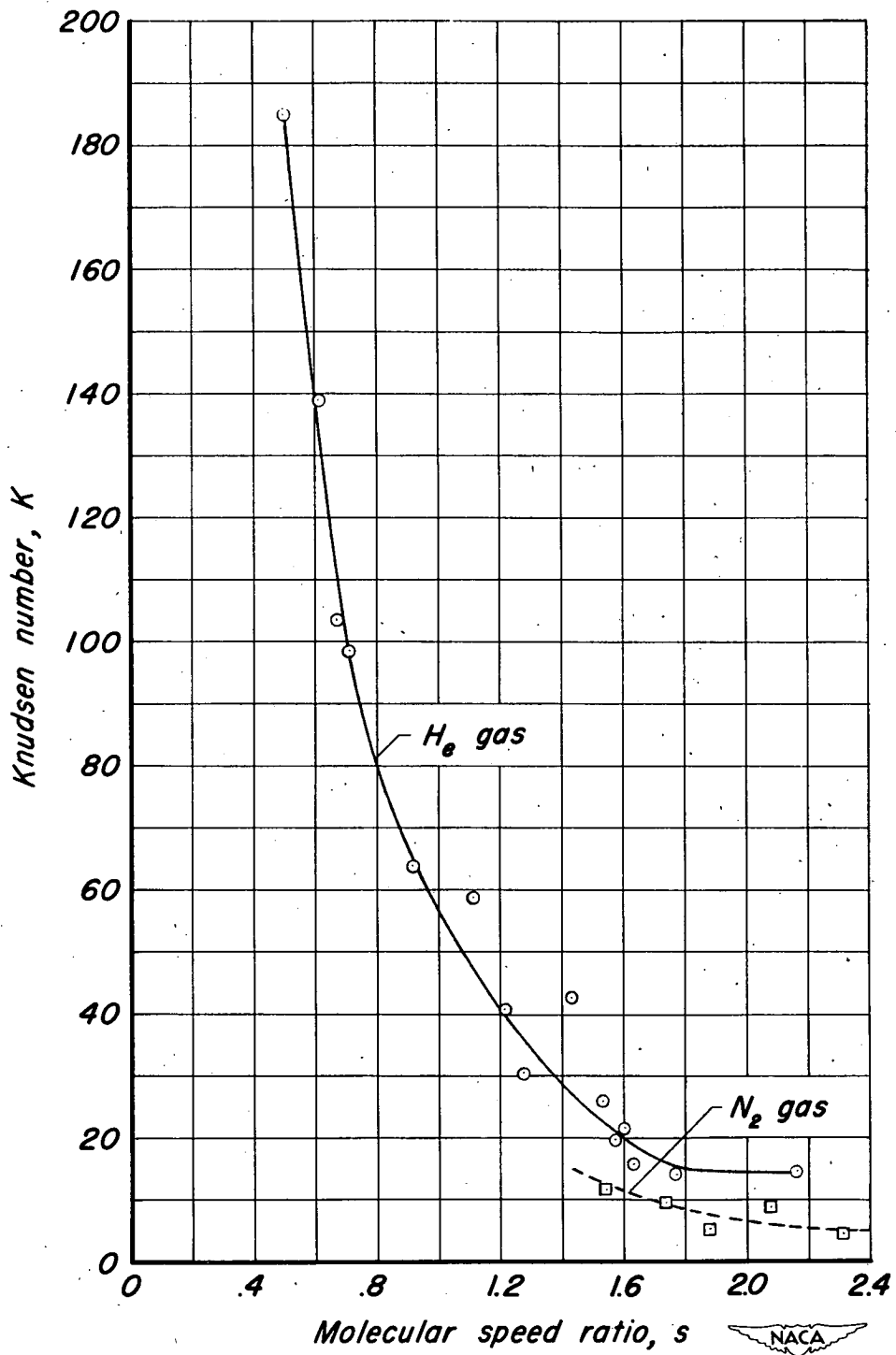Figure 22.- Variation of total drag coefficient with molecular speed ratio.

Figure 23.– The range of Knudsen numbers and molecu-
   lar speed ratios covered in the tests. Knudsen
   number based upon model radius.